

# VALIDATION AND VERIFICATION OF THE LONG-TERM DYNAMIC EVOLUTION OF NON-OPERATIONAL SATELLITES IN LEO TO ENABLE ACTIVE DEBRIS REMOVAL MISSIONS

Alain Benoit<sup>(1)</sup>, Tiago Soares<sup>(2)</sup>, Vasco Pereira<sup>(3)</sup>, Vincent Conings<sup>(4)</sup>, Estefania Padilla<sup>(5)</sup>, Enrico Melone<sup>(6)</sup>, Thomas Imhülse<sup>(7)</sup>, Martin Kruse<sup>(8)</sup>, Peter Offterdinger<sup>(9)</sup>

<sup>(1)</sup>*ABSspaceConsulting, alain@abspaceconsulting.com, alain.benoit.boutaeva@gmail.com*

<sup>(2)</sup>*ESA/ESTEC, tiago.soares@esa.int*

<sup>(3)</sup>*ESA/ESTEC, vasco.pereira@esa.int*

<sup>(4)</sup>*ESA/ESTEC, vincent.conings@esa.int*

<sup>(5)</sup>*ESA/ESOC, estefania.padilla@ext.esa.int*

<sup>(6)</sup>*ESA/ESTEC, enrico.melone@ext.esa.int*

<sup>(7)</sup>*ZARM Technik AG, thomas.imhulse@zarm-technik.de*

<sup>(8)</sup>*ZARM Technik AG, martin.kruse@zarm-technik.de*

<sup>(9)</sup>*ZARM Technik AG, peter.offterdinger@zarm-technik.de*

## ABSTRACT

In view of Active Debris Removal (ADR) missions, the observed long term dynamic evolution of defunct satellites is challenging, with often high angular rates, very far from an ideal Gravity Gradient lock. ESA is taking a proactive and innovative approach by preparing some of the future Copernicus Expansion satellites for a possible removal as part of the End-of-Life management in case they would not have successfully performed the required de-orbiting operations. These Design for Removal (D4R) technologies are being developed and matured, so that in the future they can be reliably adopted by other missions. They comprise among others a precursor Magnetic Detumbling System patented by ESA (Patent Ref EP19182205) dissipating energy by short-circuiting the on-board Magnetic Torquers; Navigation Aids to support attitude reconstruction from ground and, during the Active Debris Removal (ADR) mission itself, enable precise pose and attitude determination by the chaser.

A comprehensive analysis of spinning defunct satellites in LEO is proposed, to identify long-term dynamic drivers and guide the performance verification process of Passive Magnetic Detumbling (PMD). At system level, this process mainly relies on High-Fidelity simulations. Guidelines are proposed for the development of dedicated simulators by satellite prime contractors which shall capture the relevant phenomena, and for the simulation campaign. In parallel, an analytical framework with a simplified simulator is recommended to quickly sweep the driving parameters (S/C data and initial conditions) and guide the High-Fidelity simulation campaign.

An application example to one LEO future mission is shown, using a High-Fidelity simulator developed by ESA/ESTEC and a semi-analytical simulator prototyped by ABSpaceConsulting. This shows the added value of optimized Magnetic Torquers and the criticality of Solar Array orientation with respect to the principal axes of inertia. The analytical approach is applied to TOPEX/Poseidon dynamic evolution, complementing published papers relying mainly on simulations.

The HW validation process of short-circuited Magnetic Torquers under implementation by Copernicus Expansion missions is described, highlighting the specific approach to carry out electromagnetic measurements with extremely small induced currents and magnetic dipoles.

# 1 INTRODUCTION

ESA under the umbrella of the Clean Space Initiative is actively developing technologies and sets of requirements in view of Active Debris Removal (ADR) missions. These developments need to be accompanied by a validation and verification at system level. An Interface Requirements Document [AD1] specifies interfaces with the host satellite. The minimisation, prediction and estimation of the angular rates and attitude of non-controlled satellites to be captured is crucial for the design of the chaser and to confirm the feasibility of these critical operations. A comprehensive set of Design for Removal (D4R) technologies are therefore developed by ESA: a precursor Magnetic Detumbling System consisting in the automatic short circuiting of Magnetic Torquers; Navigations Aids consisting in Laser Retroreflectors (LRRs) to support the attitude determination from ground, 2D markers to support rendezvous from 50 m to 5 m and 3D marker to support the final metres of rendezvous; and a Mechanical Capture Interface.

One of the main challenges driving the complexity of the rendezvous and capture of a debris is that in-orbit observation of defunct satellites has shown that angular rates can build-up after satellite decommissioning as illustrated in section 2. Consequently, our current understanding of the spinning phase is shared, highlighting the impact of Gravity Gradient, Solar Radiation Pressure (YORP effect), S/C Residual Magnetic Dipole, atmospheric drag, Eddy currents and Magnetic Detumbling Systems.

Section 3 presents guidelines for the Passive Magnetic Detumbling (PMD) performance verification process. Due to the complexity of the dynamic effects, it mainly relies on extensive simulation campaigns performed on a dedicated High-Fidelity simulator. Guidelines related to the set-up of a representative, but not unnecessarily complex, High-Fidelity simulator are proposed. Analytical models based on orbit-averaged torques for a spinner have been developed by ESA and ABSpaceConsulting. They are recommended to perform sensitivity assessments and guide and correlate High-Fidelity simulations.

Section 4 presents one High-Fidelity Simulator developed internally at ESA/ESTEC and the analytical framework for the spinning phase and associated semi-analytical simulator prototype developed by ABSpaceConsulting. They are used to predict the Magnetic Detumbling Performance of a Copernicus-like mission “SAT LEO” implementing ESA ADR technologies, demonstrating the added value of optimized Magnetic Torquers and Solar Array reorientation. Analytical interpretations are shared to understand TOPEX/Poseidon dynamic evolution, complementing published papers relying mainly on simulations.

Section 5 presents Hardware level validation and verification activities. A major validation milestone is the confirmation by tests that the magnetic core is indeed excited at the very low regimes of tumbling-induced currents and the mathematical models are correct. Since the expected low inductions in the magnetic torquer are too small to be measured conventionally a three-step method was proposed by ZARM Technik and a multiple number of magnetic torquers were examined, permitting to correlate the analytical prediction of inductance, resistance and consequently the magnetic tensor. The optimisation theory of Magnetic Torquers for PMD, still respecting the operational requirements, has also been successfully tested on a dedicated prototype.

Conclusions are proposed in section 6, followed by References, Acknowledgements and Annex.

## 2 THE PUZZLING DYNAMIC EVOLUTION OF SATELLITES LEFT WITHOUT AOCS

An ideal situation for ADR would be that satellites after a successful disposal with negligible angular rates, but remaining unfortunately on a protected orbit, would converge autonomously towards a stable Earth-locked attitude thanks to the Gravity Gradient torques and energy dissipation, like happened for the Moon around the Earth.

Unfortunately, attitude reconstructions of defunct satellites reveal a variety of complex evolutions, ending up sometimes with significant angular rates. The presence on board of Laser Retro Reflector (LRR) initially designed to support demanding orbit tracking accuracy requirement and by chance not located at the center of mass, has enabled this difficult task.



*Fig. 1: Laser Retro Reflectors: precursor “Navigation Aids” in view of ADR missions*

Such observations have triggered the following considerations and actions.

- ADR design for Rendezvous and Capture shall be compatible with a tumbling or spinning non-cooperative defunct satellite and not rely on a 3-axes attitude.
- It is necessary to better understand long-term dynamics evolution of defunct satellites. The spinning configuration is the main study case to be understood and mastered.
- For future missions, in case they would be unable to perform the required end-of-life functions (e.g. failure to perform controlled re-entry due to loss of mission), dedicated features to simplify / support the rendezvous and capture for a removal service provider should be foreseen. ESA is developing a number of activities and technologies under the “Design for Removal (D4R)” terminology.

### 2.1 The challenging diversity of defunct satellites rotational motion in LEO

A sudden failure on 8 April 2012 let the 8-ton Envisat uncontrolled at 800 km altitude. The Solar Array orientation was 180 deg from the canonical position shown in Fig. 3. According to attitude reconstructions from the ground ([RD6], [RD9]) the defunct satellite has experienced a puzzling but favourable, at least so far, history. As shown in Fig. 2, after an initial spin-up during the first year, Envisat spin rate started to decrease until apparently an equilibrium around 1.5 deg/s.

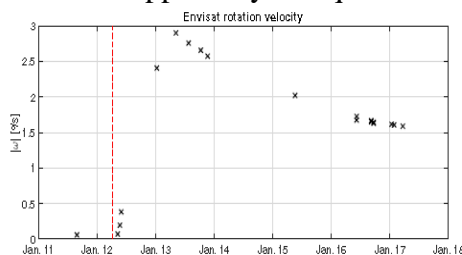


*Figure 4. Angular velocity derived by TIRA measurements from August 2011 to March 2017. The red dashed line indicates the date of loss of contact, 8 April 2012.*

*Fig. 2: The history of Envisat spin rate between 2012 and 2017 in [RD9]*

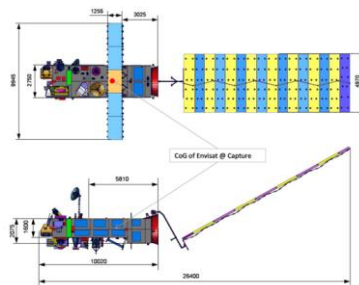


*Fig. 3: Envisat satellite configuration (Credit Airbus Defence & Space)*

TOPEX/Poseidon represents another relevant and challenging reference for dynamic analyses. Its operational orbit was a non-polar LEO with an altitude of 1336 km and inclination 66.5 degrees. It was successfully decommissioned on October 9, 2005. Attitude reconstruction on ground has shown a dramatic spin-up along the first 11 years following the end of mission, reaching around 30 deg/s as shown in Fig. 4 ([RD7])

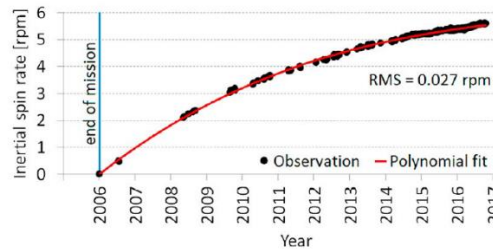


**Fig. 4: The history of TOPEX/Poseidon spin rate in [RD7]**

The satellite configuration with its single lateral Solar Array in canonical position is shown in Fig. 5. This paper will propose in section 4.4 some analytical interpretations.



**Fig. 5: TOPEX/Poseidon satellite configuration (Credit CNES)**

Follow-up JASON satellites were launched on the same operational orbit as TOPEX/Poseidon. We learn from Jason 2, decommissioned in October 2019, that a symmetrical spacecraft with 2 Solar Arrays may experience spin-up and not only Envisat or TOPEX-like spacecraft with a single lateral Solar Array. Indeed, the tumbling period reconstruction by different methods in [RD13] shows angular rates increasing from 4 deg/s to 10 deg/s over 2 years.

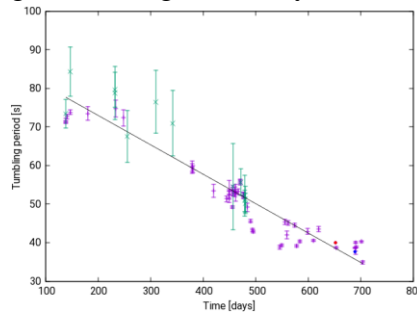


**Fig. 6: Spin period of Jason-2. Time in days from 1.1.2020 in [RD13] Observations from Graz photon counter / SLR, Zimmerwald, and TIRA**



**Fig. 7: Jason-2 satellite configuration (Credit Thales Alenia Space)**

## 2.2 Our current understanding of the spinning phase in LEO polar orbit

The following assumptions and notations will be considered for the spinning phase. It is assumed that energy dissipation has driven a flat spin transition and the satellite is spinning around its major principal axis  $Z_p$  of inertia  $I_z$ , at an angular rate  $\omega_z$  with a negligible nutation. Transverse principal inertias are  $I_x$  and  $I_y$ . The orbit is quasi-circular and quasi-polar, and the orbital rate is  $\omega_0$ . The long-term effect of an external torque  $\vec{T}$  upon the angular momentum  $\vec{H} = I_z \vec{\omega}_z$  can be predicted analytically from the spin-averaged or orbit-averaged or day-averaged external torque integrated in a quasi-inertial reference frame. This approach cannot capture the instantaneous short-term evolution of the satellite axes and nutation motion but will predict the long-term drift of the mean angular momentum over the considered period. Euler angles (precession, nutation, intrinsic rotation) are not adequate to characterise such spinning phase. What is called hereafter “precession” represents the drift of the angular momentum in an inertial frame (or quasi-inertial frame).

The view of a non-operational S/C in LEO polar orbit shown in Fig. 8 shows the common reference frame  $\mathcal{R}_{QI}$  ( $X_{QI}, Y_{QI}, Z_{QI}$ ) selected to analyse the angular momentum evolution in module and direction.

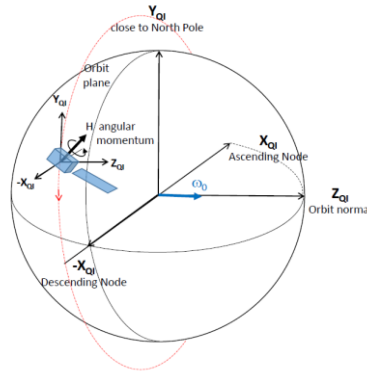


Fig. 8: Non-operational S/C on LEO polar orbit

### 2.2.1 Precession created by the Gravity Gradient torque on a spinning satellite

Observed spin rate increases cannot be produced by the Gravity Gradient torque, which is conservative and does not modify the module of the angular momentum. Its effect on a spinning body is a precession of the spin axis carrying the angular momentum around the orbit pole as shown in Fig. 9. This behaviour is similar to the well-known lunisolar precession of the Earth, responsible for the precession of equinoxes.

This is clear looking at the orbit-averaged torque expression demonstrated in [RD1]:

$$\langle \vec{T}_{GG} \rangle_{orbit} = \frac{3\omega_0^2}{2} \left[ I_z - \left( \frac{I_x + I_y}{2} \right) \right] (\vec{Z}_{QI} \cdot \vec{Z}_p) (\vec{Z}_p \times \vec{Z}_{QI}) \quad (1)$$

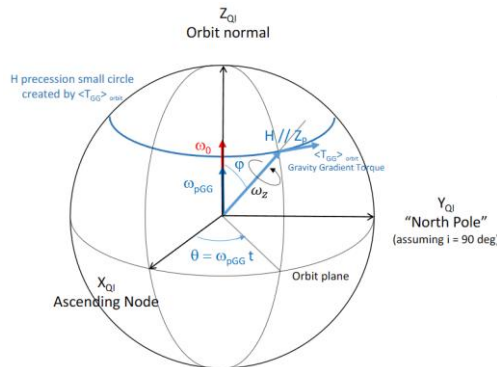


Fig. 9: Precession motion of the angular momentum around the orbit normal due to Gravity Gradient at constant obliquity in [RD1]

A remarkable result is that, should the Gravity Gradient torque be the only external disturbing torque and the spin rate large enough to maintain sufficient gyroscopic stiffness, the mean value of the obliquity angle  $\varphi$  remains constant. The period corresponds typically to several days for a spin rate of several deg/s and decreases if the spin rate decreases.

$$\omega_{pGG} = \frac{\langle T_{GG} \rangle_{orbit}}{H \sin \varphi} = \frac{3\omega_0^2}{2H} \left( I_z - \frac{I_x + I_y}{2} \right) \cos \varphi \quad (2)$$

**NOTE 1:** One important consequence of this precession motion is a variation of the sun elevation angle, which can be beneficial to limit the Sun Radiation Pressure spinning torque and/or not remain in a worst case sun illumination configuration.

**NOTE 2:** This precession motion was not reported in early papers reconstructing the spin axis direction of Envisat which was assumed inertial. Matching models shall consider it.

**NOTE 3:** There is no precession for obliquity angles 0, 90 or 180 deg.

**NOTE 4:** An inertial orbit pole was assumed. Indeed, extension to a sun-synchronous orbit shows a spiralling motion of the angular momentum, which tracks the drifting orbit pole.

### 2.2.2 Precession created by the residual dipole magnetic torque on a spinning satellite

Another significant disturbing torque in Low Earth Orbit is the magnetic torque generated by the interaction between the Earth magnetic field  $\vec{H}$  and the satellite residual dipole  $\vec{M}$ .

The simplified Earth magnetic dipole model, shown in Fig. 10 for a polar orbit, has been validated by comparison with IGRF-13 with a special care given to the Earth magnetic moment  $\mu_E$ . Its value has been fine tuned in [RD1] to  $\mu_E = 7.763 \cdot 10^{15} T \cdot m^3$  in order to get for a polar orbit the same orbit-averaged value of the squared norm  $\langle \|\vec{B}\|^2 \rangle_{orbit}$ , which drives long-term Passive Magnetic Detumbling. In Eq. (3) the magnitude of the satellite radius vector  $r$  is expressed in meters.

$$\vec{B} = B_{eq}(-2 \sin \theta \vec{u}_r + \cos \theta \vec{u}_\theta) \quad (3)$$

$$B_{eq} = \frac{\mu_E}{r^3} \quad (4)$$

$$\langle \|\vec{B}\|^2 \rangle_{orbit} = \frac{5}{2} B_{eq}^2 \quad (5)$$

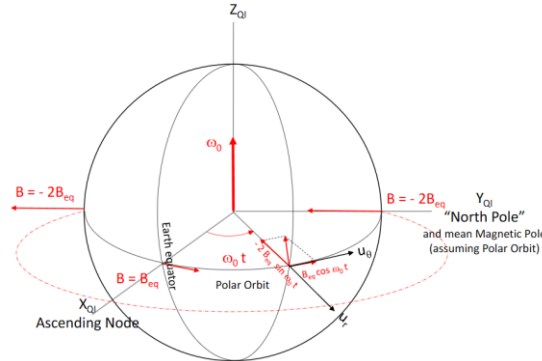


**Fig. 10: Earth magnetic field dipole model along a polar orbit**

Only the component  $\mathcal{M}_{RDZ}$  along the spin axis  $Z_p$  creates a non-null mean torque over one spin period: Considering now the orbital motion on a polar orbit, the orbit-averaged torque is given in [RD1] by:

$$\overrightarrow{\langle T_{RD} \rangle}_{orbit} = \frac{\mathcal{M}_{RDZ} B_{eq}}{2} (\overrightarrow{Y_{QI}} \times \overrightarrow{Z_p}) \quad (6)$$

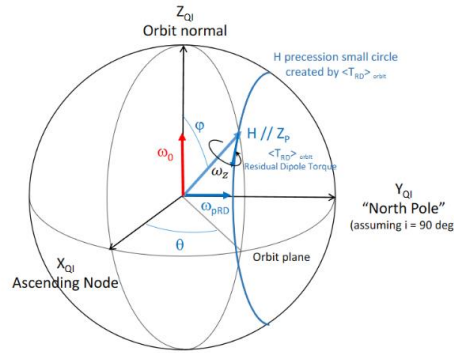


**Fig. 11: Precession motion of the angular momentum around the North Pole due to Residual Dipole in [RD1]**

The torque created by the satellite magnetic residual dipole torque causes the spin axis to precess in a cone around the Earth Pole at a precession rate  $\omega_{pRD}$  which only depends on the spin rate and not on the angle  $\alpha$ .

$$\omega_{pRD} = \frac{\langle T_{MD} \rangle_{orbit}}{H \sin \alpha} = \frac{\mathcal{M}_{RDz} B_{eq}}{2H} \text{ if } \alpha \neq 0 \quad (7)$$

**NOTE 1:** Combined with the GG precession, this torque will produce small oscillations of the obliquity angle, with sometimes rapid evolutions when the angular momentum crosses the orbit plane (obliquity 90 deg).

**NOTE 2:** Values around 10 to 15 Am<sup>2</sup> per axis can be considered as typical values for medium size satellites.

*Pre-flight measurements are recommended to support the prediction of in-orbit evolution.*

### 2.2.3 Impact of the aerodynamic torque

For the Earth observation missions, especially at low altitudes the aerodynamic forces and torques may represent a significant disturbing factor for the orbital and attitude dynamics.

For a satellite with a single lateral Solar Array, a rough estimation of the aerodynamic torques acting on the spinning spacecraft with a single solar array can be assessed.

In the spinning motion the solar array sweeps the circular motion over the centre of rotation. During the first half of revolution the spin induced tangential velocity decreases of the relative velocity, whereas during the second half of revolution the relative velocity increases. The spin-averaged aerodynamic torque tends to negligible or even to have a small rate damping effect.

**NOTE:** Current knowledge is that this torque has a negligible impact during the spinning phase.

*It might positively contribute to some stabilisation if and after the angular rates have been damped below typically 0.2 deg/s.*

### 2.2.4 Impact of Solar Radiation Pressure

SRP torques created by the presence of large lateral Solar Arrays are generally recognised as the primary source of non-conservative torques able to spin-up or temporarily spin-down a defunct satellite. Satellite decommissioning should consider this effect.

As reported in [RD2], even if a Solar Array is ideally oriented in a canonical position with respect to the geometrical axes, the spin axis unbalance linked to the cross products of inertia, will create a tiny repetitive accumulation of momentum contributing to the YORP effect (named after Yarkovsky–O'Keefe–Radzievskii–Paddack).

This phenomenon is illustrated in Fig. 12. with a cross product of inertia  $I_{xz}$ , creating a misalignment  $\varepsilon_y$  around  $Y_G$  between the spin axis  $Z_P$  and the body axis  $Z_G$ . Such misalignment creates slight but repetitive variations of the sun incidence angle on the front and back sides of the Solar Array.

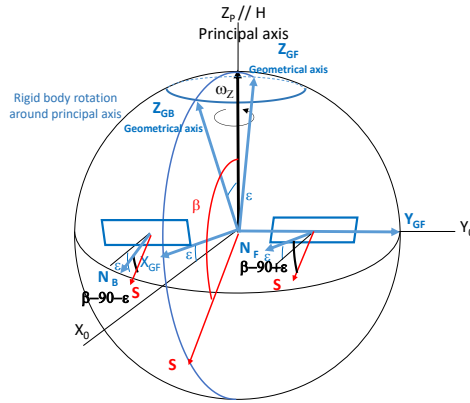


**Fig. 12: Impact of misalignment  $\epsilon_y$  (from Cross-Product of Inertia  $I_{xz}$ ) in [RD2]**

The zoom shown in Fig. 13 clearly shows the torque dissymmetry over a spin revolution created by the spin axis misalignment.

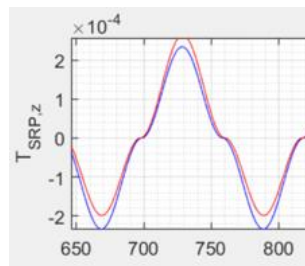


**Fig. 13: Torque profiles over one spin period in [RD3]  
blue: w/o spin axis unbalance  $\langle Tz \rangle = 0$   
red: with spin axis unbalance  $\langle Tz \rangle \neq 0$**

If the sun elevation  $\beta > 90^\circ$ , the Solar Array back side is more lit than the front side and creates a negative spinning torque.

If the  $\beta < 90^\circ$ , the Solar Array front side is more lit than the back side and creates a positive spinning torque.

The spin-averaged SRP torque  $\overline{\langle T_{SRP} \rangle}_{spin}$  directly depends on the sun elevation angle.

A map can be generated in the Reference Frame attached to the Angular Momentum, taking due consideration of the principal axis misalignments. Analytical expressions have been developed by ABSpaceConsulting. Such map can also be generated with Hi-Fi simulations, but on a case-by-case basis as shown in Fig. 28 for TOPEX/Poseidon (with selected thermo-optical coefficients of the Solar Array front and back sides and its orientations wrt the principal spin axis)

Fig. 14 shows an example for a single Solar Array close to the optimised position  $\alpha$  recommended by ESA in [AD1], aiming at compensating the principal axis misalignment  $\epsilon_y$  around Y such that  $\alpha - \epsilon_y \sim 0$ . In case of perfect compensation, there is no spin-averaged SRP torque:  $\langle T_{SRP} \rangle_{spin} = 0$ .

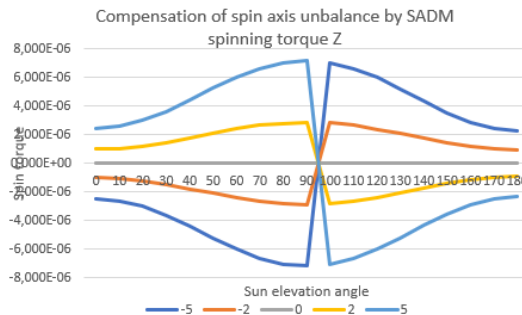


**Fig. 14: Spinning torque versus elevation angle beta for different Solar Array orientations wrt spin principal axis**

A sharp discontinuity is experienced when the sun elevation crosses the spinner equator ( $\beta = 90^\circ$ ). This is generally experienced by defunct satellites, even in sun-synchronous orbit, due to the precession of the angular momentum created by the Gravity Gradient torque. The value and sign of the long-term mean SRP torque will depend on this complex history as shown in Fig. 15. SRP tilting torques can also be created, but they are in most cases dominated by the Gravity Gradient torque.



**Fig. 15: The sun elevation history generates an alternative profile for the SRP spinning torque with an uncertain mean value**

**NOTE 1:** The SRP spinning torque will compete with the PMD damping torque and the outcome is difficult to predict. The PMD damping torque is proportional to the spin rate. The SRP spinning torque depends on the sun elevation. If a stable repetitive pattern of sun elevation is reached, the asymptotic spin rate will correspond to an equilibrium between both torques.

**NOTE 2:** In addition to the direct SRP torques, the torques created by the IR thermal reemission of the surfaces heated by the sun must be considered. The impact can be neglected if the temperature gradient between the front and back sides of the Solar Arrays are small and if their emissivities are close.

### 2.2.5 Passive Magnetic Detumbling Systems

In order to damp the angular rates, kinetic energy dissipation means are necessary.

Eddy currents have been recognised as the source of angular rates damping on a number of tumbling satellites or launcher upper stages.

A complementary solution, taking advantage of equipment already on board of LEO satellites was proposed by ESA through the short-circuiting of the satellite Magnetic Torquers ([RD4] ESA patent Ref EP19182205). The tumbling motion of satellites within the Earth magnetic field results in the induction of currents in their coils, dissipating energy by Joule heating and damping the satellite angular rates facilitating the Rendezvous and capture by an Active Debris Removal mission.

In the new end of mission use, the 6 coils of the 3 Magnetic Torquers would be automatically short-circuited.

$$\overrightarrow{T}_{PMD} = - \left[ M \left( \frac{d\vec{B}_{Earth}}{dt} \right)_{sat} \right] \times \vec{B}_{Earth} = - [M(-\vec{\omega} \times \vec{B})] \times \vec{B} - \left[ M \left( \frac{d\vec{B}}{dt} \right)_{inertial} \right] \times \vec{B} \quad (8)$$

As explained in [RD1], [RD2] assuming a pure spin rate  $\omega_z$  around the S/C principal axis  $Z_p$  (no nutation), a simple Earth magnetic dipole model with a module  $B_{eq}$  at Equator, and a Magnetic tensor with 3 equal components  $M$ , the orbit-averaged Passive Magnetic Detumbling torque acting on a spinner on a polar orbit is:

$$\langle \overrightarrow{T}_{PMD} \rangle_{orbit} = -M \frac{5}{2} B_{eq}^2 \begin{pmatrix} \frac{11}{20} \omega_z \sin \varphi \cos \theta \\ \frac{11}{20} \omega_z \sin \varphi \sin \theta \\ \omega_z \cos \varphi - \frac{9\omega_0}{5} \end{pmatrix}_{\mathcal{R}_{Q1}} \quad (9)$$

The projection along the spin axis shows two components: a “rotational” component predominant at high angular rates and vanishing if the satellite becomes inertial and an “orbital” component smaller but which remains present due to the Earth magnetic field evolution in quasi polar LEO even if the S/C angular rates have vanished.

$$\dot{H} = (T_{XQI} \cos \theta + T_{YQI} \sin \theta) \sin \varphi + T_{ZQI} \cos \varphi = -M \frac{5}{2} B_{eq}^2 \left[ \omega_z (1 - 0.45 \sin^2 \varphi) - \frac{9\omega_0}{5} \cos \varphi \right] \quad (10)$$

**NOTE 1:** Launchers upper stage with mainly conductive structure are prone to develop Eddy currents and a large magnetic tensor.

**NOTE 2:** Considering the most prominent conductive elements of a typical Copernicus satellite (full Aluminum walls, conductive layers of CFRP elements and Titanium tanks assumed to be spherical), the diagonal values of the Eddy currents magnetic tensor as estimated by ESA typically lie in the range  $0.3 \cdot 10^4 \Omega^{-1} m^4$  to  $6.5 \cdot 10^4 \Omega^{-1} m^4$ .

**NOTE 3:** The magnetic tensors of the AOCs Magnetic Torquers, when both coils are short-circuited, are estimated to be in the range  $2.0 \cdot 10^4 \Omega^{-1} m^4$  to  $2.0 \cdot 10^5 \Omega^{-1} m^4$

A damping torque is always present as long as the spin rate is sufficiently high. Tilting components modify this orientation, but for a given obliquity  $\varphi$ , and if there is no Sun Radiation Pressure secular torque, the short-term evolution of the spin rate is an exponential decay with an instantaneous time constant  $\tau(\varphi)$  expressed in Eq. (12) for a polar orbit.

$$\omega_z(t) \sim \omega_{z0} e^{-t/\tau(\varphi)} \quad (11)$$

$$\tau(\varphi) = \frac{I_z}{M \frac{5}{2} B_{eq}^2 (1 - 0.45 \sin^2 \varphi)} \quad (12)$$

A reference time constant  $\tau_0$  appears, directly related to the Magnetic Tensor parameter M, the spin inertia  $I_z$  and the module of the Earth magnetic induction at equator  $B_{eq}$ .

As shown above, this minimum time constant corresponds to an angular momentum parallel or anti-parallel to the orbit normal. The time constant increases in a ratio 1 to around 2 with the obliquity angle  $\varphi$ .

$$\tau_0 = \frac{I_z}{M \frac{5}{2} B_{eq}^2} \quad (13)$$

The factor  $\frac{5}{2} B_{eq}^2 (1 - 0.45 \sin^2 \varphi)$  corresponds to  $\langle \|\vec{B}_\perp\|^2 \rangle_{orbit}$  derived from the Earth magnetic field dipole model on a polar orbit. It is important to take note that, if not superseded by competing

tilting torques, the “orbital” component  $\langle \vec{T}_{PMD2} \rangle_{orbit} = M \frac{5}{2} B_{eq}^2 \begin{pmatrix} 0 \\ 0 \\ \frac{9\omega_0}{5} \end{pmatrix} \mathcal{R}_{QI}$  will bring the angular

momentum parallel to the orbit pole as shown in Fig. 16 ([RD1], [RD2]). This might explain in-orbit observations.

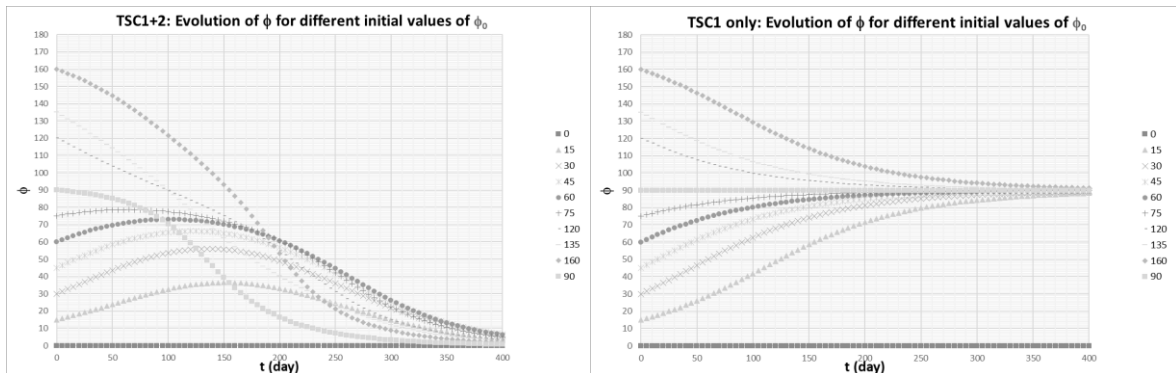


**Fig. 16:** The orbital component of the PMD tilting torque brings the obliquity to 0 deg (left) and not 90 deg (right)

### 3 SYSTEM LEVEL PERFORMANCE VALIDATION AND VERIFICATION

Due to the complexity of the SRP effect and the low authority of current Passive Magnetic Detumbling Systems (short-circuited Magnetic Torquers and Eddy currents), an extensive simulation campaign performed on a dedicated High-Fidelity simulator is necessary to assess the PMD (Passive Magnetic Detumbling) performance.

Constraints are very different from classical AOCS/GNC simulators where continuous closed loop does not require very long-term dynamics accuracy. Papers addressing the prediction of defunct satellites dynamic evolution generally present Very-High-Fidelity simulators which capture and model all astrodynamics and environmental phenomena, and the associated CPU time is detrimental to run for instance Monte-Carlo simulations. It is desirable to find the adequate approach, and not systematically run heavy models and features which have negligible effects.

ESA intends to prepare a Technical Memorandum providing useful information to the space systems developers community on the specific subject of Magnetic Detumbling performance validation and verification. A preliminary collection of guidelines for the verification approach is listed in Section 3.2, with guidelines related to the High-Fidelity simulator in section 3.1.

#### 3.1 Passive Magnetic Detumbling (PMD) performance verification approach

The following guidelines are proposed. They should be considered as preliminary; updates will be welcome using lessons learnt from different actors and instantiations.

a. The PMD performance verification should be performed through numerical simulations on the PMD High-Fidelity simulator

b. Dedicated analyses should be undertaken to identify driving parameters

*NOTE 1: Critical parameters in case of lateral Solar Arrays are the Thermo-Optical parameters of front and back faces, their Infrared thermal emission and their misalignments*

*NOTE 2: A semi-analytical simulator is recommended to quickly check the impact upon long term dynamics*

c. The selected approach for simulations should be defined and justified

*NOTE 1: Analytical framework can guide the simulation campaign definition*

*NOTE 2: The approach can use for instance Monte Carlo method with 2 sigma confidence level*

*NOTE 3: It is recommended to perform first a series of simulations, focusing on driving parameters affecting the detumbling performance*

*NOTE 4: Simulations should not be stopped as soon as the angular rates fall below a certain value, an apparently successful detumbling can be ruined by spin up/spin down following cycles*

d. Analyses should be undertaken to promote a good interpretation of the results

*NOTE 1: Correlation with analytical formulas during the spinning phase is expected: Gravity Gradient precession period, reference time constant, map of SRP spin-averaged torque versus sun elevation, etc.*

*NOTE 2: A detailed interpretation of simulation results is expected to give confidence in long term stabilization of the angular rates*

*NOTE 3: Correlation with semi-analytical simulator results is recommended for cross-validation*

e. Relevant S/C and orbit parameters should be gathered, including at least the following elements:

Orbital parameters of the spacecraft at mission end of life

Spacecraft Mass, Centering, Full Inertia Matrix parameters at the end of mission life

Thermo-optical characteristics of the surfaces in solar and infrared spectrum at EOL

Estimations or preferably measurements of spacecraft residual magnetic dipole

Estimation of the overall spacecraft magnetic tensor including Magnetic Detumbling System and Eddy currents

Definition of realistic range of parameters (including assumed distribution)

f. Relevant initial conditions should be defined, covering in particular the following elements:

Angular rate vector, Obliquity, Local Time of Ascending Node, Epoch, and consequently sun elevation

Solar Array(s) orientation(s) and other appendages configuration

### 3.2 Setup of PMD High Fidelity Simulator

The following guidelines are proposed. They should be considered as preliminary; updates will be welcome using lessons learnt from different actors and instantiations.

- a. The PMD High-Fidelity simulator should be representative of:
  1. Satellite dynamics and kinematics of interest for Passive Magnetic Detumbling.
  2. Space environment related to the dynamic evolution of attitude and orbital position.
  3. The Magnetic Detumbling System generating magnetic torques.
- b. The identification of specific features to be represented or not in the S/C dynamics and the space environment simulation shall be justified and documented with the associated mathematical models.

*NOTE 1: Section 2.2 and 4.2 of this paper can guide this identification exercise.*

*NOTE 2: Rigid body dynamics is generally representative enough for PMD performance assessment.*

*NOTE 3: 3<sup>rd</sup> body gravitational interactions are expected to have negligible impact.*
- c. The simulation model of the Magnetic Detumbling System should be validated with respect to the real hardware behaviour characterized in a representative environment.

*NOTE 1: Such characterisation test is generally done by the unit supplier on highly specialized test benches.*

*NOTE 2: Complementary end to end verification of PMD System efficiency could be done by the prime on a dynamic test bench.*
- d. Verification and validation of the entire simulator should be performed using functional test cases.

*NOTE 1: Section 2.2 of this paper can provide several test cases.*

*NOTE 2: The generation of orbit-averaged torques to be compared with analytical formulas is a strong contribution for functional validation.*

*NOTE 3: It is desirable to enable and disable specific modelled phenomena using appropriate parameter flags such that individual effects of the detumbling dynamics can be studied.*
- e. Adequate numerical integration methods and settings for long duration open-loop simulation should be selected.

*NOTE 1: Artefacts such as fake nutation damping or increase, or sun elevation drift should be eliminated.*

*NOTE 2: Integration time step size is particularly critical.*
- f. It should be possible to run Monte-Carlo simulations with the parametric ranges and distributions.
- g. The PMD High-Fidelity simulation environment should offer extensive capabilities for a dedicated post-processing and data analysis.

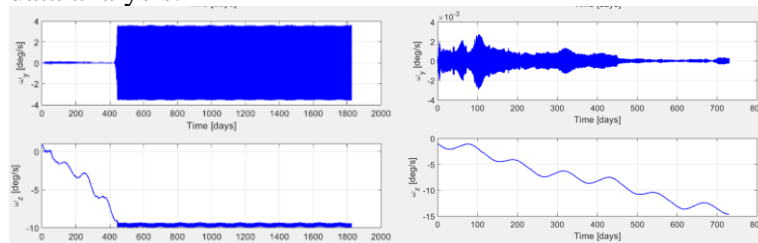


**Fig. 17: Impact of integration step size: left 10 s and right 1s (fixed)  
Fake nutation increase (left) and correct dynamics (right)**

### 3.3 Added value of a supporting analytical framework

In-orbit observations have shown that ADR design for Rendezvous and Capture shall be compatible with a tumbling or spinning non-cooperative defunct satellite and not rely on a 3-axes attitude.

The spinning configuration has therefore appeared as the main study case to be understood and simulated. An analytical framework based on spin-averaged and orbit-averaged torques has been developed by ESA and ABSpaceConsulting. It is instrumental to interpret the complex behaviour shown in-orbit or by the simulations, identify S/C driving parameters and representative initial conditions, and sweep parameters accordingly. Application example will be shown in section 4.3.

This analytical framework is the detailed development of the fundamental phenomena presented in section 2.2. It can be either used as is when analytical solutions of differential equations exist, or incorporated in a semi-analytical simulator which calculates not anymore the 3-axes instantaneous dynamic evolution but the mid-term and long-term evolution of the angular momentum and spin axis direction, as shown in section 4.2.

## 4 SIMULATION EXAMPLES

### 4.1 ESA/ESTEC High-Fidelity simulator

To perform detailed analyses on spacecraft attitude dynamics and kinematics during Passive Magnetic Detumbling scenarios, a High-Fidelity simulator is required. This simulator needs to accurately capture the attitude motion of passive satellites in space, while simultaneously requiring low computation effort. Therefore, it should only implement the spatial environment that is relevant to the dynamic evolution of the attitude and position of resident space objects. Details on the High-Fidelity simulator that has been developed by ESA/ESTEC and used for the current paper are discussed below.

#### 4.1.1 Space Environment

The space environment block of the simulator implements the environmental surroundings encountered by a passive spacecraft in orbit. In particular, as the current implementation of this High-Fidelity simulator limits its applicability to spacecraft in near-vicinity of Earth, the following models are implemented:

- A solar ephemeris model
- A solar radiation pressure model
- A conical eclipse model
- An Earth rotation model
- A zonal gravity model of Earth up to and including J6
- An IGRF13 magnetic field model
- An exponential atmosphere model

These environment models pertain to the Sun and the Earth and represent the relevant models for Passive Magnetic Detumbling scenarios. Further models, such as third-body gravitational attraction, Earth albedo and Earth infrared radiation or an atmospheric wind model are considered of secondary importance and are omitted to improve computational efficiency.

#### 4.1.2 Satellite Model

The satellite model provides the interface between the environmental models and the dynamic evolution of the passive satellite state. It is implemented as a rigid-body model since flexible effects would not have any meaningful effects on the passive spacecraft. Furthermore, this rigid body model contains a simplified shape model, implementing a rectangular grid with appropriate thermo-optical properties. An example representation of such a satellite model is given in Fig. 21.

#### 4.1.3 Magnetic Detumbling System Model

Specific to Passive Magnetic Detumbling scenarios is the calculation of the torques generated by the short-circuited magnetic torquers. A model for these torques has previously been provided in Eq. (8). Characteristic to this equation is the magnetic tensor of the short-circuited torquers, as this has a direct relation with the detumbling performance. The higher this tensor, the faster the torquers can detumble the passive spacecraft. Additionally, also the Eddy current torque generates a detumbling effect on the passive spacecraft, as it generates a torque opposite to the spin direction. It can be modelled using the same equation as for the short-circuited magnetic torquers. Note that these passive magnetic damping torques are modelled as disturbances acting to the satellite attitude dynamics.

#### 4.1.4 Satellite Dynamics and Kinematics

The satellite dynamics and kinematics model contains the equations of motion that are integrated to obtain the motion evolution of the passive satellite in space. Therefore, it implements the following acceleration and torque models:

- Gravitational acceleration of Earth

- Gravity gradient torque of Earth
- Residual magnetic dipole torque in geomagnetic field
- Solar radiation pressure torque
- Aerodynamic drag torque
- Eddy current torque in geomagnetic field
- Short-circuited magnetic torquer torque in geomagnetic field.

These acceleration and torque models pertain to the Sun, the Earth and the spacecraft and represent the minimum disturbances that need to be modelled from the previously discussed spatial environment.

Note that, on top of providing a correct parameterisation of the models provided above, a compelling post-processing of the results is required. As such, to obtain a more intuitive insight on the disturbance torques net-effect on the rate evolution of the passive spacecraft spin-averaging, orbit-averaging or even day-averaging can be performed.

Furthermore, the setup of the High-Fidelity simulator incorporates Monte Carlo functionality, allowing to swiftly perform a parameter sweep of the input settings. This is because the performance of Passive Magnetic Detumbling is highly dependent on the initial conditions, such as the Solar Array orientation, while simultaneously containing a high uncertainty of the spacecraft properties at end-of-life, e.g., the thermo-optical properties of the spacecraft surface. Therefore, a Monte Carlo analysis provides a statistically founded metric for the Passive Detumbling Performance of a given satellite. Moreover, the High-Fidelity simulator has been designed with a predefined simulation time, rather than implementing a stopping condition triggered when the angular velocity norm dives under a given threshold value, for example. This is because not all damping profiles are stable, as will be discussed in Section 4.3 and subsequent spin-up phases would not be detected.

This further implies that long simulation times are required to have confidence in a stable damping profile, which leads to the implementation of an efficient numerical solver to reduce computation time, while still ensuring sufficiently small integration time step.

## 4.2 ABSpaceConsulting semi-analytical simulator

The basic principles presented in section 2.2 applied to LEO quasi-polar orbits have been further studied by ABSpaceConsulting.

The analytical framework for the spinning phase has been progressively developed and documented in Technical Notes delivered to ESA with some published elements in [RD1], [RD2]. A supporting semi-analytical simulator is useful to integrate orbit-averaged torques with a typical time-step between 0.1 and 1 day and provide a preliminary assessment of the evolution of the spin rate, obliquity and sun elevation, and comprehensive plots of the various torques driving the dynamic evolution.

The quasi-inertial reference frame  $\mathcal{R}_{QI}$  shown in Fig. 18 is used to express the various torques.

The angular momentum is referenced by its module  $H$  and the two angles  $(\varphi, \theta)$  as shown in Fig. 18.

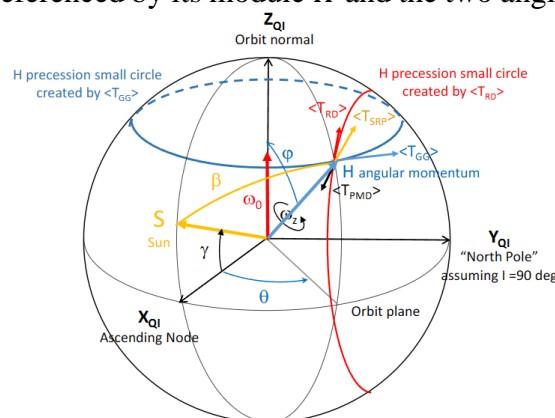


Fig. 18: Quasi-inertial reference frame  $\mathcal{R}_{QI}$

The fundamental equations of evolution are summarized in Annex. A semi-analytical simulator prototype has been coded, with several simplifications to remain “Excel-friendly”.

The SRP torque is only calculated for the Solar Array (no central body faces, no shadowing effects). The quasi-inertial reference frame is considered as inertial: non precessing quasi-polar orbit and fixed sun direction. This is not detrimental for a Copernicus Expansion mission on a sun-synchronous orbit since the angular momentum tracks the orbit normal thanks to the Gravity Gradient precession and the LTAN remains constant. The tilting components of the SRP torque are not computed for any Solar Array orientation, but only when their normal is close to the principal axis.

More general equations could be coded in a more flexible environment.

The reduced number of data sufficient to define the spinning phase is shown in Table 1. They cover physical constants, mission and satellite data, initial conditions, activation flags to enable/disable the various torques and integration step size.

It is extremely easy to modify any parameter and see in a couple of seconds the impact on dynamic evolution.

**Table 1**

Magnetic Damping	Magnetic tensor MTQ	1,484000E+05	Orbit	Orbit altitude (km)	750
	Magnetic tensor Eddy currents	3,680000E+03		Tday/Torbit	0,647
Mag. Dipole	S/C Residual Dipole Z	12,00	Principal inertia	X principal inertia (kg.m2)	1500,00
Geom axis misalign	SA misalign. (alpha-epsilon)Y	5,00		Y principal inertia (kg.m2)	2000,00
	SA misalign. (epsilon)X	-1,74		Spin inertia Iz (kg.m2)	2600,00
IR Flag	Flag = 0 (SRP only) or 1 (SRP + IR)	0	Single Solar	Solar Array area	7,250
Front side optical coeff	$C_{a1}^F$	0,88	Back side optical coeff	Solar Array lever arm	3,710
	$D_{a1}^F$	0		$C_{a1}^B$	0,84
	$C_{s1}^F$	0		$D_{a1}^B$	0
	$D_{s1}^F$	0,12		$C_{s1}^B$	0
Physical constants	Initial conditions	initial spin rate (deg/s)	3	Earth radius (km)	6378
		phi0 (obliquity)	80,00	Earth gravity GM	3,99E+14
		theta0 (azimuth)	90,00	Earth magnetic moment (T.m3)	7,763E+15
		gamma (sun,node)	20,00	Solar flux	0,00000465
Activation flags for each torque					
Flag GG	Flag RD	Flag MTQ	Flag SRP	Flag Aero	
1	1	1	1	NA	

The simulation results are no longer valid if the spin rate falls below typically 0.5 deg/s. Characteristics such as the reference time constant, the initial Gravity Gradient precession period, and the map of the SRP spin component map shown in Fig. 19 are automatically computed.

A lot can be understood when visualizing the evolution of the orbit-averaged torques as shown in Fig. 20, such as the authority of the Passive Magnetic Detumbling with respect to the spinning component of the Solar Radiation Pressure when the spin rate and the sun elevation evolve.

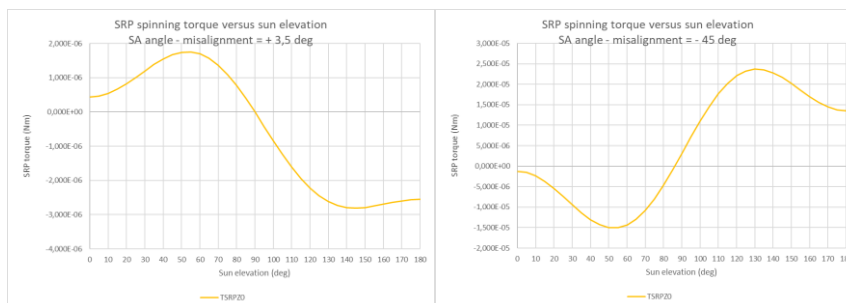


**Fig. 19: Map of SRP spinning torque versus sun elevation for 2 Solar Array orientations wrt spin axis: 3.5 deg (left) and -45 deg (right)**

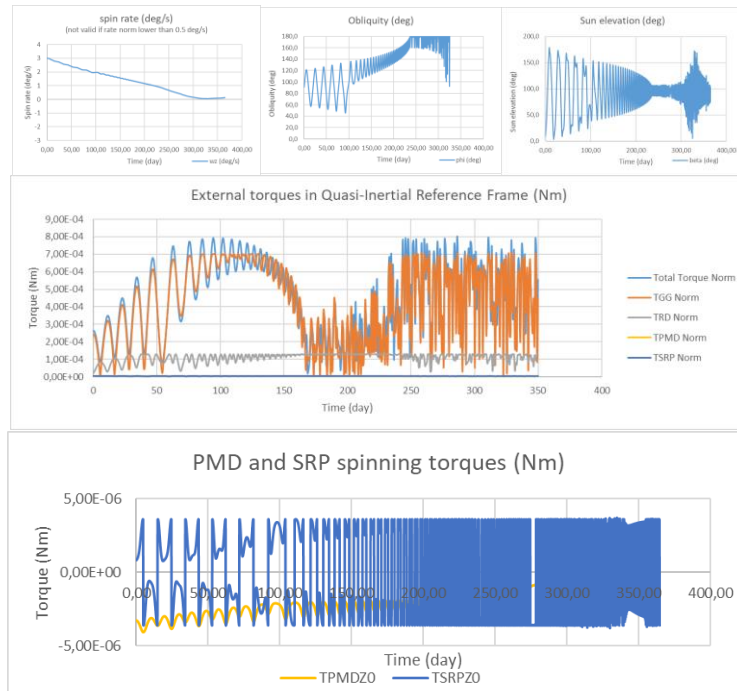


**Fig. 20: Results from semi-analytical simulations**

### 4.3 Application to SAT LEO

This section outlines the various steps of a performance verification process of Passive Magnetic Detumbling (PMD) for SAT LEO, a fictitious satellite in Low Earth Orbit prepared for ADR.

**ESA SDM Standard requirement (in preparation):**

**The Satellite design shall implement the following functions**

- Enable attitude reconstruction from ground,
- Limiting and damping the satellite angular rates,
- Guarantee access to a mechanical interface for capture,
- Passively aid to servicer relative navigation

**NOTE: The target accuracy of attitude reconstruction from ground should be  $\ll 1$  deg/s and the evolution of the module of the satellite angular rates vector should converge to values lower than 1 deg/s.**

SAT LEO configuration with one lateral Solar Array is shown in Fig. 21 and its main characteristics for PMD performance verification including uncertainties are listed in Table 2.

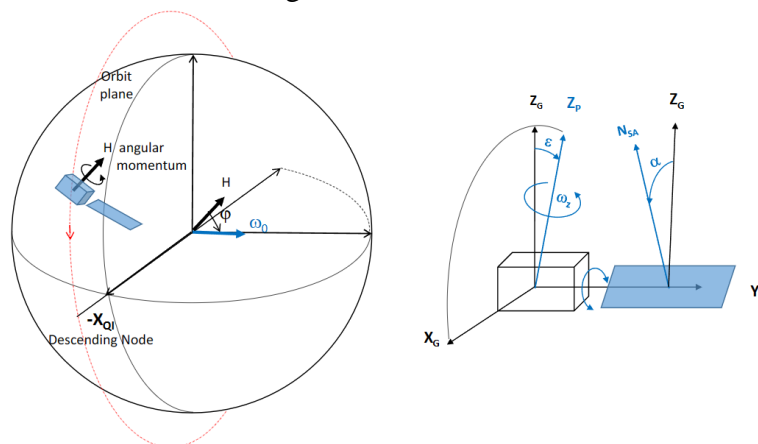


**Fig. 21: SAT LEO configuration**

**Table 2: SAT LEO relevant parameters for Passive Magnetic Detumbling**

Simulation Parameter	SAT LEO
Orbit altitude (km)	640
Orbit inclination	Sun synchronous
LTDN	12h30
Principal Moments of Inertia [ $I_x, I_y, I_z$ ] (kg. m <sup>2</sup> )	[1000,800,1300] ±5%
Misalignments of major principal axis $Z_P$ wrt geometrical axis $Z_G$	$ \varepsilon_y  \leq 3.5^\circ$ around $Y_G$ and $ \varepsilon_x  \leq 3.5^\circ$ around $X_G$
S/C residual magnetic dipole (A.m <sup>2</sup> ) (max. values)	[±10, ±10, ±10]
MTQ Magnetic Tensor $M_1$ (Ω <sup>-1</sup> m <sup>4</sup> )	[2.7, 2.7, 2.7] × 10 <sup>4</sup>
Optimized MTQ Magnetic Tensor $M_2$ (Ω <sup>-1</sup> m <sup>4</sup> )	[7.75, 7.75, 7.75] × 10 <sup>4</sup>
Future PMD system Magnetic Tensor $M_3$ (Ω <sup>-1</sup> m <sup>4</sup> )	[7.75, 7.75, 7.75] × 10 <sup>5</sup>
Eddy currents Magnetic Tensor (Ω <sup>-1</sup> m <sup>4</sup> )	[1.25, 1.25, 1.25] × 10 <sup>4</sup>
Solar array (SA) area (m <sup>2</sup> )	7.0
CoG to SA center of pressure offset (m)	[0, 3.5, 0]
SA front side specular reflection coefficient	~0.0
SA front side diffuse reflection coefficient	~0.12
SA back side specular reflection coefficient	~0.0
SA back side diffuse reflection coefficient	~0.84
Aerodynamic drag coefficient	2.3

### 4.3.1 Preliminary assessment

The analytical framework and semi-analytical simulator can be used to perform a first assessment of the detumbling performance, starting with a feasibility analysis and trade-off selection of the Passive Magnetic Detumbling system.

#### a) Feasibility analysis:

- Variation of the magnetic tensor  $M$  of the selected Magnetic Detumbling System
- Variation of the Solar Array orientation (with reference to the principal axis  $Z_P$ )

The inertia matrix is selected to present a misalignment of -3.5 deg of the major principal axis around the Solar Array rotation axis.

$$I = \begin{pmatrix} 1000 & 0 & -18.42 \\ 0 & 800 & 0 \\ -18.42 & 0 & 1300 \end{pmatrix}$$

For this feasibility analysis, the initial obliquity is selected as 20 deg, and the S/C Residual magnetic dipole as 0 A.m<sup>2</sup>. Different Solar Array orientations are tested, generating the following spin-averaged SRP torque along the spin axis, with respect to the sun elevation:

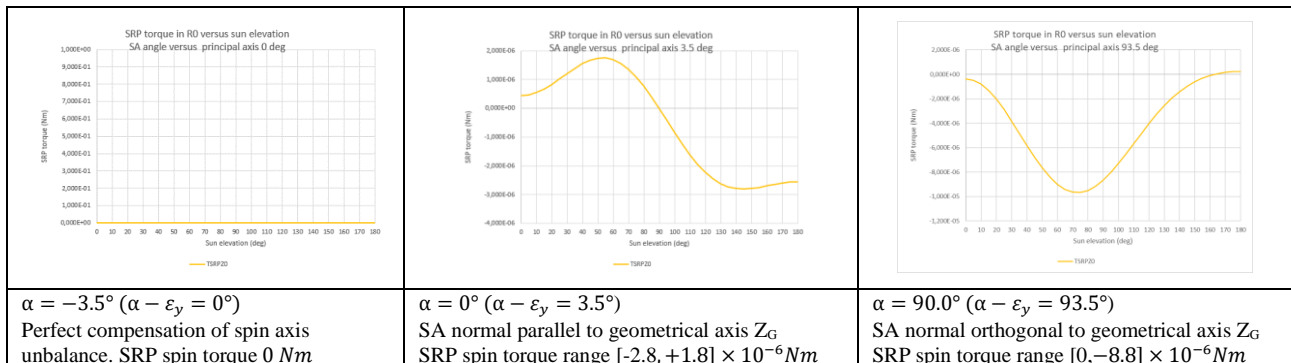


**Fig 22: Map SRP spinning torque versus sun elevation for the Solar Array orientations of Case #1, Case #2 and Case #3**

**Table 3: Magnetic Tensors and Solar Array Orientations for feasibility analysis**

	PARAMETERS			RESULTS		
	Magnetic Tensor	Solar Array orientation		$\tau_0$ (day)	$\omega_z$ (°/s) After 1 year	COMMENTS
		$\alpha$ (°)	$\alpha - \varepsilon_y$ (°)			
#1	$M_1$	-3.5	0	302	1.06	SRP spin torque is cancelled
#2	$M_1$	0	3.5	302	1.33	SRP spin/despin torque
#3	$M_2$	0	3.5	133	0.45	SRP spin/despin torque
#4	$M_2$	90.0	93.5	133	-3.5	Permanent SRP despin torque
#5	$M_3$	90.0	93.5	15	-0.5	Permanent SRP despin torque

Fig. 23 shows the evolution of the spin rate provided by the semi-analytical simulator with an integration step size equal to 0.03 day.

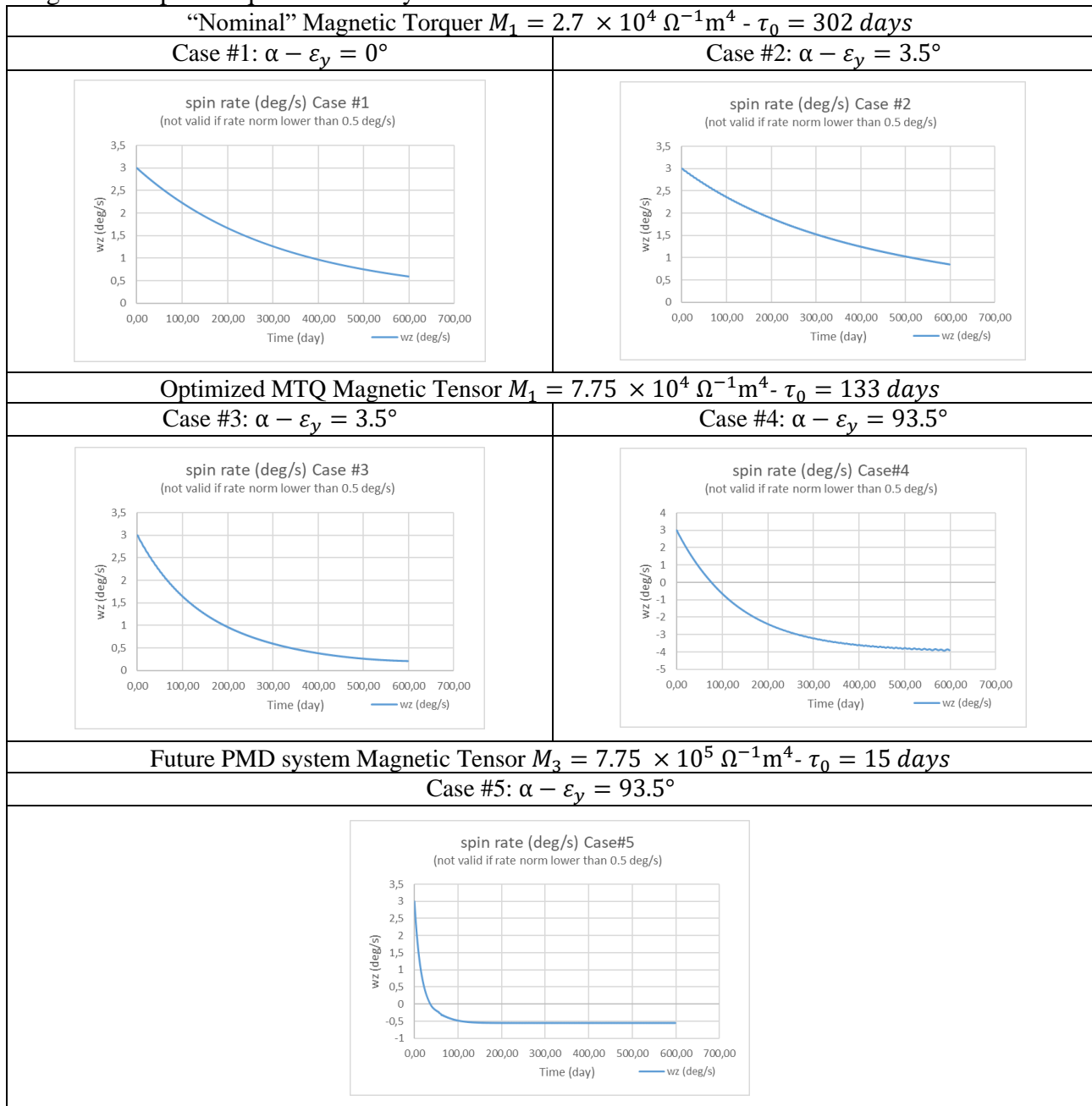


**Fig. 23: Spin rate profiles with semi-analytical simulator**

Case #3 appears a good candidate to fulfil ADR requirements and the baselined Magnetic Detumbling System is the optimised MTQ. It is recommendable to guarantee a specific SA orientation with respect to the major principal axis. However, this would require a precise knowledge of the principal axis direction, which is not obvious. An intermediate approach consists in ensuring that the SA normal is parallel to the geometrical axis, i.e. in canonical orientation  $\alpha = 0$  deg, and to live with the balancing uncertainties  $|\varepsilon_y| \leq 3.5^\circ$  around  $Y_G$ .

**b) Sensitivity analysis with case #3:**

The semi-analytical simulator allows to quickly sweep parameters, like the obliquity angle, the S/C residual magnetic dipole, etc.

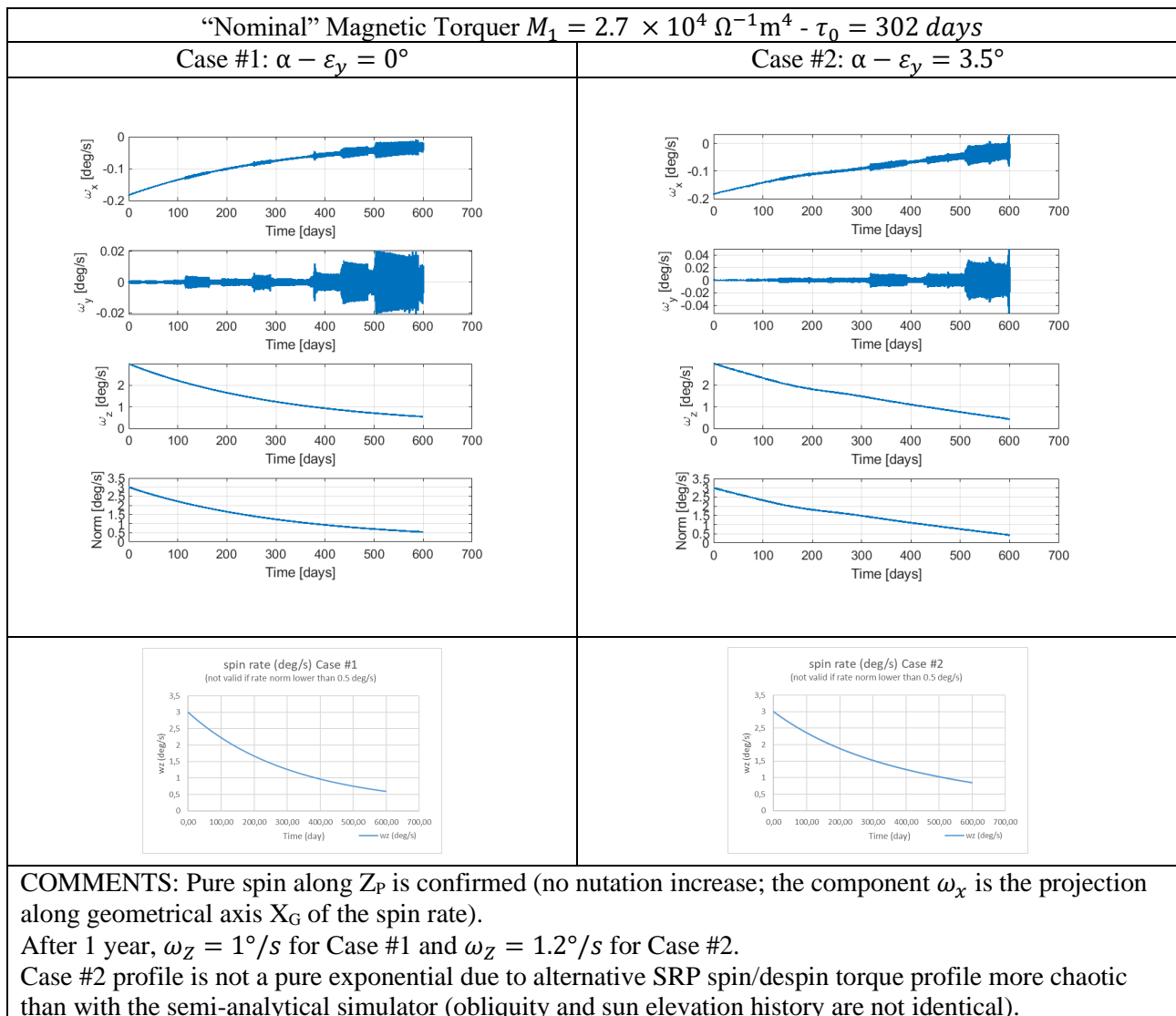
- Variation of the obliquity angle  $\varphi$ : between 0 and 180 deg
- Impact of the S/C residual magnetic dipole along  $Z_G$ : +10, -10
- etc

The spin rate behaviour appears to be very similar, and the next step can be performed.

**4.3.2 Confirmation by Hi Fi simulation**

**a) Initial correlation with the feasibility analysis assessment**

Fig. 24 shows the 3 angular rates in S/C geometrical axes provided by the Hi-Fi simulator for cases #1 to #5, using a variable step integrator with relative and absolute tolerances equal to  $10^{-7}$ .



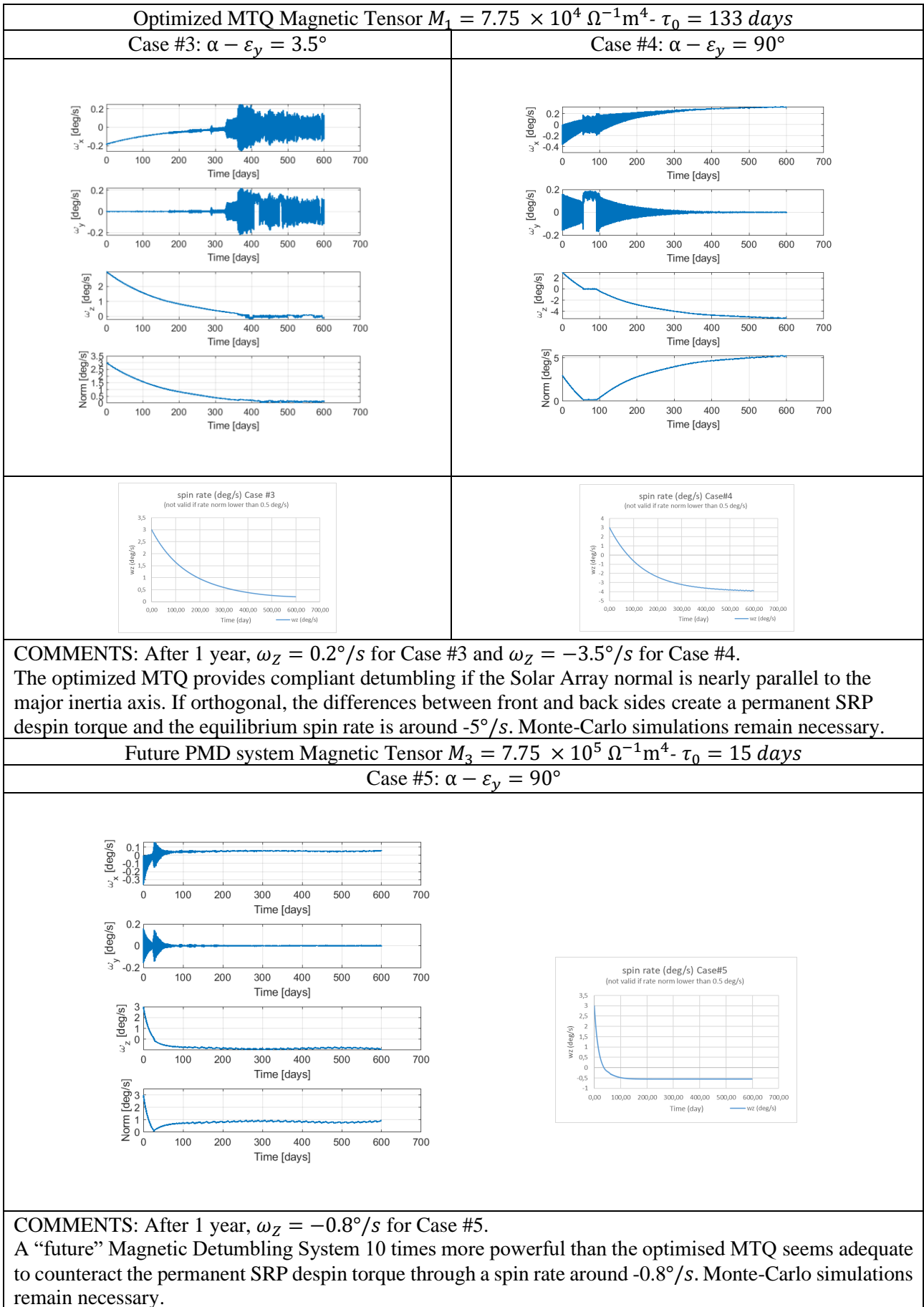


Fig. 24: Angular rates profiles with Hi-Fi simulator

High-Fidelity simulations correlate reasonably well with the rough assessment performed by the simplified semi-analytical simulations. They provide a first insight regarding transverse rates during the spinning phase and the follow-up low-rate tumbling phase.

The baselined case 3 seems to be confirmed for the next step.

More insight could be brought by considering the SRP maps in Fig 22 and the various profiles in Fig. 20 (obliquity, sun elevation, SRP torque). If a mean long term SRP torque  $\langle T_{SRP} \rangle_{long\ term}$  can be estimated from these profiles, the stabilised spin rate will correspond to the equilibrium between this torque and the PMD torque: As long as the satellite remains spinning around its major principal axis the following equation applies:

$$\langle T_{Z_0}^{SRP} \rangle_{long\ term} - M \frac{5}{2} B_{eq}^2 \left( \omega_z \cos \varphi - \frac{9\omega_0}{5} \right) = I_z \dot{\omega}_z = 0 \quad (14)$$

$$\omega_z^\infty = \frac{\langle T_{Z_0}^{SRP} \rangle_{long\ term}}{\frac{5}{2} M B_{eq}^2 \cos \varphi} + \frac{9\omega_0}{5 \cos \varphi} \quad (15)$$

### 4.3.3 Monte-Carlo campaign

Following this comprehensive analysis of driving phenomena and parameters, a reduced Monte Carlo campaign for SAT LEO has been performed, for this paper a quick exercise limited to 50 cases, 600 days and variations of initial spin rate (between 0 and 5 deg/s), CoG position, inertia tensor and thermo-optical coefficients.

The following statistics was obtained: norm of the angular rates below 1 deg/s: 44% (22) (see Fig. 25), norm below 1.5 deg/s: 78% (39) and norm below 1.75 deg/s: 88% (44).

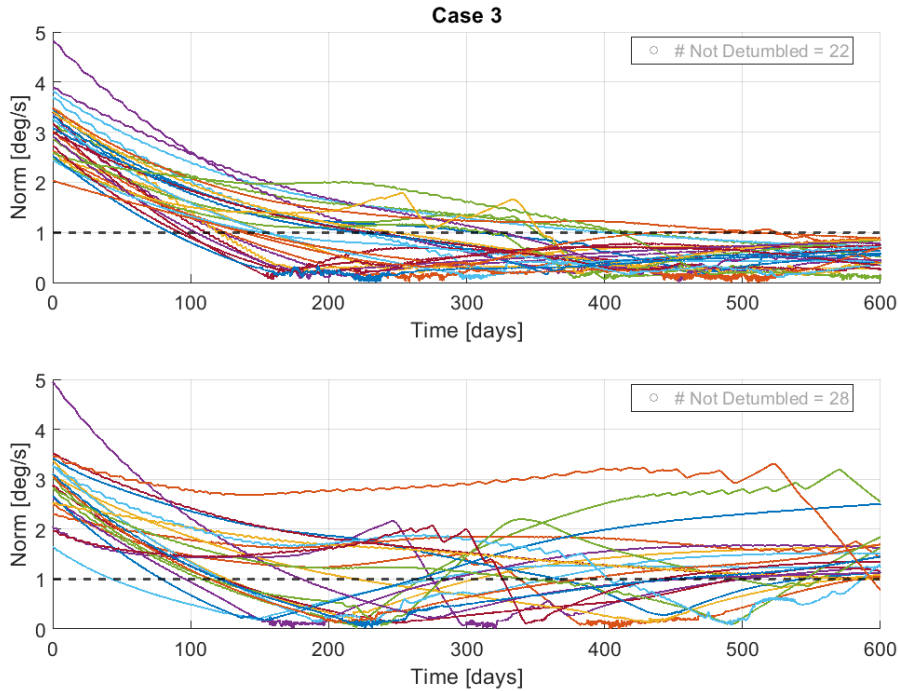


**Fig. 25: 44% cases below 1.0 deg/s and 78% below 1.5 deg/s**

The spin-down phase seems correct except 3 outliers. It would then be necessary to gain confidence regarding stabilization through a detailed examination of the following tumbling phase. A real project would finally consider whether relaxed performances are acceptable, or revisit the Magnetic Detumbling System selection, or revisit Solar Array orientations or S/C characteristics.

#### 4.4 Some analytical contributions to understand TOPEX/Poseidon dynamic evolution

TOPEX/Poseidon is one important reference case, having shown that large angular rates can appear after a successful decommissioning.

Several papers ([RD7], [RD8], [RD12]) have successfully reproduced the spin rate evolution, by High-Fidelity simulations. Such identification exercise is however delicate, especially when important driving parameters like S/C inertias and Solar Array orientation are not known.

No equivalent simulation effort can be offered in this section, but instead contributions based on analytical interpretation of TOPEX/Poseidon dynamic evolution. This was not the scope of this paper and this section does not have the pretention to be conclusive but intends to help other researchers in a collaborative effort.

The spin rate reconstruction in Fig. 4 from [RD7] shows meaningful features:

- a) a remarkably regular and smooth evolution, showing a characteristic exponential pattern.
- b) an asymptotic limit for the angular rate  $\omega_s^\infty$

This looks like the signature of a permanent spinning torque, in competition with a damping torque created by Eddy currents. Such pattern is easily modelled by a very simple macroscopic equation:

$$\langle T_{SRP} \rangle_{long\ term} + \langle T_{PMD} \rangle_{long\ term} = I_s \dot{\omega}_s \quad (16)$$

Passive Magnetic Detumbling torque in polar orbit can be extrapolated to an inclined orbit by recomputing:

$$\langle \overrightarrow{T_{SC1D}} \rangle_{orbit} = -MB_{eq}^2 \vec{\omega}_z \frac{1}{T_{orbit}} \int_0^{T_{orbit}} \|\vec{B}_\perp\|^2 dt \quad (17)$$

Eq.(14) becomes:

$$\langle T_{SRP} \rangle_{long\ term} - MB_{eq}^2 \frac{5}{2} \left[ \sin^2 i - 0.5 \sin^2 \varphi \left( 1 - \frac{9}{5} \cos^2 i \right) \right] \omega_s = I_s \dot{\omega}_s \quad (18)$$

Assuming that the obliquity is close to zero (spin axis parallel to the orbit normal) and that the mean SRP torque is reasonably constant, the spin rate evolution would be:

$$\omega_s = (\omega_{s0} - \omega_s^\infty) e^{-t/\tau} + \omega_s^\infty \quad \text{with } \tau = \frac{I_s}{2.10 MB_{eq}^2} \quad \text{and } \omega_s^\infty = \frac{\langle T_{SRP} \rangle_{long\ term}}{2.10 MB_{eq}^2} \quad (19)$$

With these assumptions, the dynamic evolution of the angular momentum could be as shown in Fig. 26 with the angular momentum tracking the precession of the orbit pole in a spiraling motion.

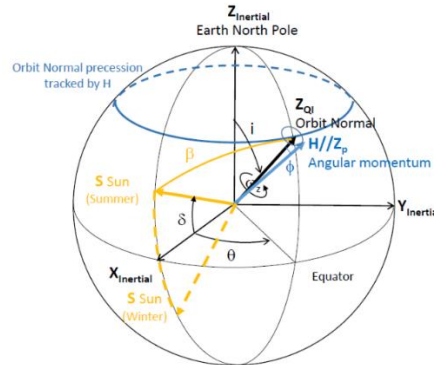


Fig. 26: Possible dynamic motion of TOPEX/Poseidon

It is easy to find parameters matching the reconstructed spin history of Fig. 4:

$$\omega_s = (\omega_{s0} - 39^\circ/s) e^{-t/5.8\ years} + 39^\circ/s \quad (20)$$

TOPEX/Poseidon inertias are apparently not known from recent authors but they can be found in Fig. 3 of [RD11]:

$I_x = 6912 \text{ slug-ft}^2 = 9371 \text{ kgm}^2$ ;  $I_y = 3107 \text{ slug-ft}^2 = 4213 \text{ kgm}^2$  and  $I_z = 8604 \text{ slug-ft}^2 = 11665 \text{ kgm}^2$

Assuming that TOPEX/Poseidon is spinning around its major principal axis, the magnetic tensor of Eddy currents can be derived:

$$M = \frac{I_z}{2.10 B_{eq}^2 \tau} = 10.5 \times 10^4 \Omega^{-1} m^4 \quad (21)$$

The value of the mean SRP torque is given by:

$$\langle T_{SRP} \rangle_{long\ term} = 39 \frac{\pi}{180} 2.10 M B_{eq}^2 = 4.0 \times 10^{-5} Nm \quad (22)$$

A simulation has been performed with ESA/ESTEC High-Fidelity simulator. The Solar Array orientation has been taken from [RD7] at 285 deg (75 deg with our convention), the magnetic tensor of Eddy currents at  $10.5 \times 10^4 \Omega^{-1} m^4$  and the reliable inertias from [RD11]. The initial obliquity was set at zero, the initial spin rate at 1 deg/s around the major principal axis.

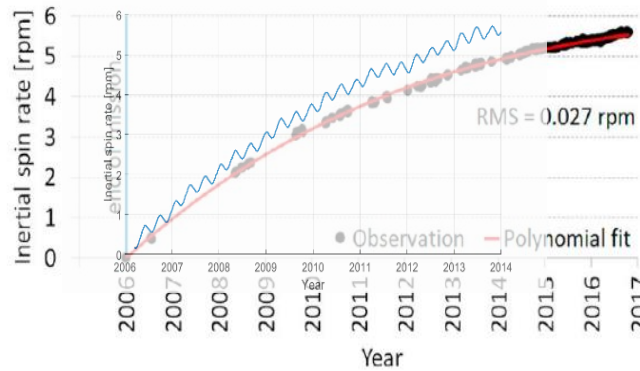


**Fig. 27: Hi-Fi simulation does not perfectly match in orbit observation**

It seems that either the detumbling torque of Eddy currents is less efficient or the SRP spinning torque generated by the simulator is too high and not equivalent to  $4.0 \times 10^{-5} Nm$ . An interesting post-processing allows to validate the analytical map SRP torque versus sun elevation for this Solar Array orientation as shown in Fig. 28.

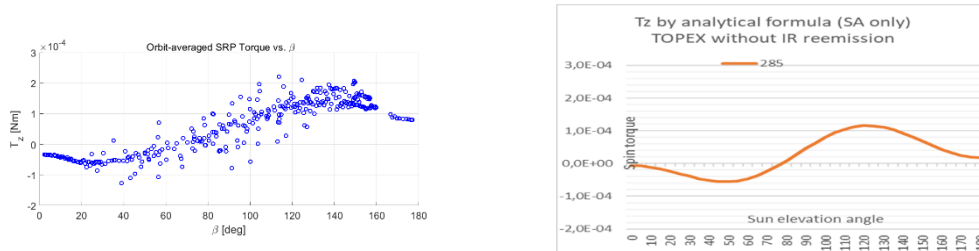


**Fig. 28: SRP orbit-averaged torque post-processing confirms the analytical model map**

This was a priori far from obvious, looking at the diversity of the maps in Fig. 29 shown for a variety of Solar Array orientations. It would be interesting to apply the time history of the sun elevation to these maps and check whether there would be other Solar Array orientation candidates equally suitable to provide a mean torque equal to  $\langle T_{Z_0}^{SRP} \rangle_{mean} = 4.0 \times 10^{-5} Nm$ . This angle would be the Solar Array orientation with respect to the major principal axis and not the geometrical axis.

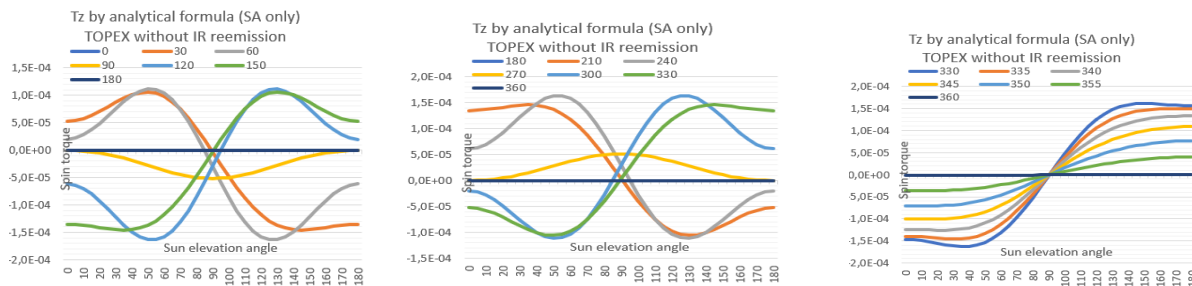


**Fig. 29: Spinning torque versus sun elevation angle for various Solar Array orientations**

About TOPEX/Poseidon inertias, precursor simulations in [RD8] did not model Eddy currents damping torque and estimated a spin inertia as large as 70 000 kg m<sup>2</sup>. This large virtual value corresponds indeed to the slope of the spin rate evolution if ignoring the Eddy current damping term as visualised in Fig. 30.

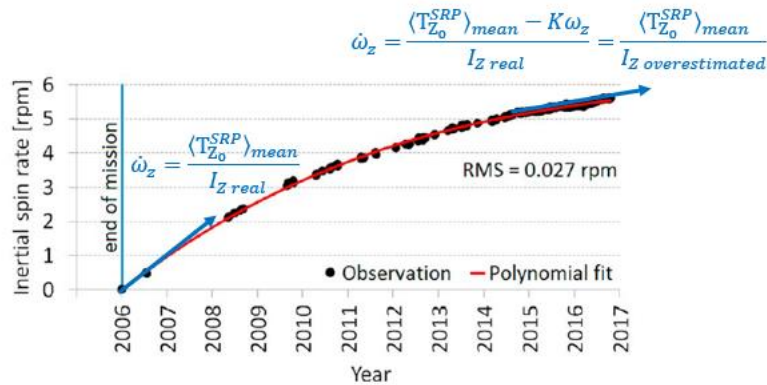


Fig. 30: Ignoring Eddy currents damping, spin inertia becomes overestimated

## 5 VERIFICATION AT HW LEVEL OF PASSIVE MAGNETIC DETUMBLING SYSTEMS

Previous analyses and simulations rely on mathematical models of the on-board Passive Detumbling System. Taking the example of short-circuited Magnetic Torquers, this section will illustrate how the concept and the mathematical models have been validated at HW level by ZARM Technik and ESA.

### 5.1 Confirmation of the magnetic core excitation at low regime:

Several tests were conducted to measure the induced coil currents in different short-circuited magnetic torquers exposed to a slowly rotating magnetic field. The first achievement of these tests conducted by ZARM Technik in collaboration with ESA is the confirmation of the magnetic core excitation at low regime (i.e. at slow rotation of the spacecraft within the Earth's magnetic field). Several torquers with a dipole moment of 250 to 400 Am<sup>2</sup> were used as test objects. The generation of a rotating magnetic field to simulate a rotation of the coils in the Earth's magnetic field has been implemented using a Helmholtz coil system.

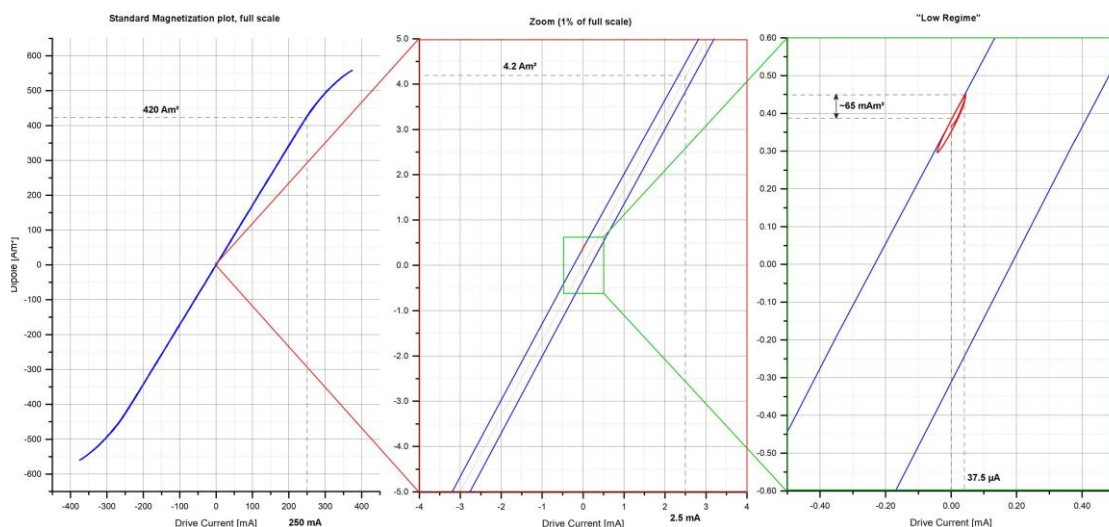


Fig. 31: 2-step zooming of Magnetic Moment  $\mathcal{M}$  versus Current  $i$ : the magnetic core is correctly excited at low regime as shown by the slope of the small hysteresis loop in [RD16]

The dramatic 2-step zooming in Fig. 31 shows the huge difference between operational regime and the very low regime of Passive Magnetic Detumbling. We can see the small hysteresis loop created by the low regime. The slope shows that the relative permeability is similar to the core permeability at operational regime. The magnetic core offers an extremely low and favourable coerciveness of about  $40 \text{ mA/cm} = 4 \text{ A/m}$ . The Earth magnetic strength in LEO is  $H_{eq} = \frac{B_{eq}}{\mu_0} = 17.5 \text{ A/m}$ .

This gives confidence that the linear model used so far in the simulation should be applicable and that the following expressions for the magnetic tensor of 2 short-circuited coils are equivalent:

$$M = \frac{2 \mu_{rod}^2 N_{turn}^2 A_{core}^2}{R} = \frac{2 L^2}{\mu_0^2 R} \left( \frac{l_{rod}}{N_{turn}} \right)^2 = \frac{2 \cdot \mathcal{M}(i)^2}{R i^2} \quad (23)$$

This result was the instrumental and successful milestone to validate the short-circuited Magnetic Torquers concept, by confirming that the magnetic core was excited also at very low regime. If not, the MTQ would create induced currents as a simple air-coil without magnetic core, i.e.  $\mu_{rod} = 1$  and its magnetic tensor would vanish in the ratio  $\mu_{rod}^2 \sim 90\,000$  with the rod permeability dropping to 1. This was further proven by ZARM testing a MTQ without magnetic core. The induced current was 176 times smaller than with a magnetic core, and the derived magnetic tensor 42 800 times smaller.

## 5.2 Test approach designed by ZARM Technik:

Since the expected low inductions in the magnetic torquer are too small to be measured conventionally, a three-step test approach has been designed by ZARM Technik:

1. Measurement of induced current in 3D Helmholtz
  - Compensated magnetic field of earth.
  - Add field of desired orbit
  - Rotate that field with constant angular rate ( $6^\circ - 3^\circ/\text{sec}$ )
  - Measure induced current with pico-amperemeter.
2. Measurement in special lab at ZARM Technik AG
  - Sinusoidal excitation in normal power mode
  - Measure behaviour of the dipole moment
3. Low current measurement
  - Sinusoidal excitation with low current of step 1 (narrow distance)
  - Compare behaviour of 2. and 3. to decrease the error.

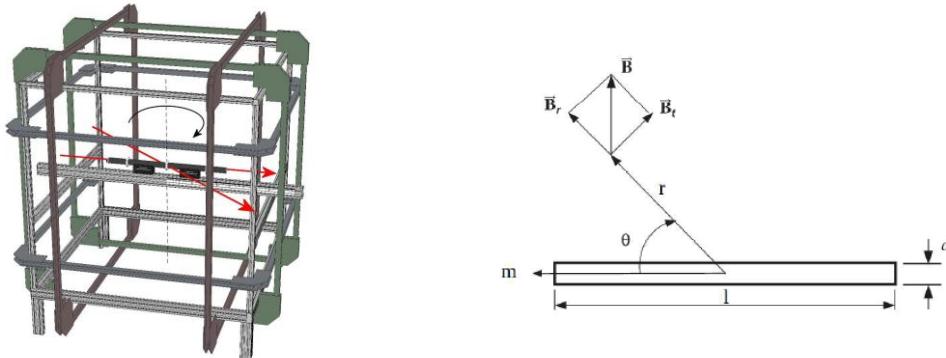


**Fig. 32: Helmholtz coil generating representative rotating field (with Earth field compensation) (left)  
Magnetic moment  $\mathcal{M}$  is derived from the measurement of  $B_r$  and  $B_t$  (right)**

In order to confirm the linearly scalable excitation of the magnetic core, even in the expected low regime, it is necessary to carry out dipole measurements with very small supply currents on the test object. As a consequence, the need of an appropriate measuring system with low sensitivity and a proper test approach is considered fundamental. In one of the first tests, a magnetic torquer optimised for ESA was placed by ZARM in a 3D Helmholtz coil configuration. With this set-up, the 2 coils were short-circuited and immersed in a magnetic field of constant magnitude  $100 \mu\text{T}$  rotating around

Z axis at 3 deg/s. This is a very low regime, however not fully representative of in-flight conditions (4 to 5 times larger than  $B_{eq}$  in LEO:  $B_{eq} \sim 2.2 \times 10^{-5} T$ ).

ZARM has measured and/or derived the following parameters, through highly sensitive test facilities and well-designed test approaches:

Classical electrical parameters:

- The resistance of 1 coil, the inductance of 1 coil, with the other one in open circuit or closed.
- The time step response (electrical time constant) of 1 coil, either with the other one in open circuit or in closed circuit. In the latter case, the time step response is nearly double due to the mutual inductance.

Innovative tests for Passive Magnetic Detumbling:

- The very low current induced by a rotating external magnetic field in short-circuited coil(s) (single coil, series, parallel).
- The dipole (magnetic moment) created by a sinusoidal current of larger magnitude.
- The dipole (magnetic moment) created by a very low sinusoidal current, calculated from the created magnetic field strength (B) measured at a small distance from the MTQ to produce measurable effects. The objective is not to get quantitative results, but to verify if the dipole behaviour is coherent with the previous one and if so, to extrapolate the previous results.
- The magnetic tensor, derived from the magnetic moment.

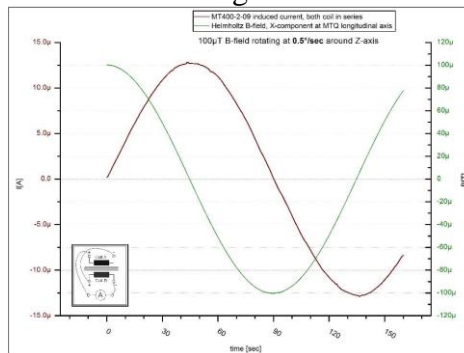


Fig. 33: Induced currents created by a rotating magnetic field

### 5.3 Application to single coil, both coils connected in series or in parallel:

Several tests have been conducted in different configurations on a custom torquer optimized for PMD. 3 main different short-circuiting configurations have been investigated: single coil, both coils in series, coils connected in parallel. These tests were performed to find a direct relation between the dipole measurement and the magnetic tensor  $M = m/\omega B$  and to confirm the good relation between the ESA model theoretical values and the real hardware measurements.

Table 4: Magnetic Tensor measurement of the optimized torquer by ZARM Technik AG

MT400-2-D21071301	B [ $\mu T$ ]	$\omega$ [ $^\circ/s$ ]	$M \pm \Delta M$ [ $m^4S$ ]	Experiment: $M_x = \frac{m_x}{B_y \omega_z}$	M ESA [ $m^4S$ ] $M = \frac{2L^2}{\mu_0^2 R} \left(\frac{l}{N}\right)^2$
Single coil	100	6	$93210 \pm 2980$		95100
Single coil	50	6	$92620 \pm 3060$		
Coils connected in parallel	100	6	$93210 \pm 2940$		
Coils connected in parallel	50	6	$93210 \pm 2980$		
Coils connected in parallel	100	3	$93790 \pm 3000$		
Average M $\pm$ 0.525%			$93208 \pm 489$		95100
Error estimates of measurements:			$\Delta m = 0.05\% - \Delta B = 3.00\% - \Delta \omega = 0.1\%$		

The induced effects are mainly linear to the magnitude and the angular velocity of the rotating magnetic field. Shorting both redundant windings generate corresponding currents of the same magnitude in both windings as well. The effects at series connection and parallel connection are basically equivalent. The nature of the housing material has no direct influence on the currents induced in the coil assembly due to the rotation. However, Eddy current effects within a conductive housing might lead to additional detumbling effects. The magnetization behaviour of the ferromagnetic core in the "low regime" is basically comparable to its magnetization within the nominal linear operating range. The significantly increased effects on the breadboard model confirm the approach of choosing the largest possible coil length and an extended L/R time constant for PMD optimization.

It is remarkable that a small error in the measurement and modelling of the PDMs leads to large deviation of the magnetic tensor and detumbling simulation. So, it becomes clear the importance of an accurate MTQ model combined with reliable laboratory tests.

#### 5.4 Quantitative correlation between analytical predictions and test results for 2 MTQ's:

Last part of the investigation was correlating Zarm MT400-2-09 and MT400-2-D21071 MTQs test results with ESA mathematical models. For these tests both coils were connected in parallel and short-circuited through an Amperemeter which measures therefore the total current, sum of the individual currents flowing in each coil.

Here we will focus our attention on the MT400-2-D21071 with CFRP non-conductive housing which has an improved behaviour for detumbling application.

*Table 5: test results and (between brackets) predictions in several short-circuiting configurations*

<b>MT400-2-D21071301</b>	$B_{test}$ ( $\mu T$ )	$\omega$ ( $^\circ/s$ )	$i$ ( $\mu A$ )	$\mathcal{M}$ ( $Am^2$ )	$\mathcal{M}/i$
Single coil	100	6	159 (166.4)	0.488 (0.502)	3069
Single coil	50	6	79 (83.2)	0.242 (0.251)	3063
Coils connected in parallel	100	6	318 (332.8)	0.976 (1.004)	3069
Coils connected in parallel	50	6	159 (166.4)	0.488 (0.502)	3069
Coils connected in parallel	100	3	160 (166.4)	0.491 (0.502)	3069

The test results confirmed the validity of the predictions based on Chen rod permeability ([RD15]) The quantitative predictions of the currents and the magnetic moments are very well correlated with the test results. The slope  $\mathcal{M}/i$  is constant and the test results confirm the validity of the mathematical models. The resistance as measured by ZARM (193  $\Omega$ ) is 1.7% larger than the model prediction (189.8  $\Omega$ ) with a value of the piling up factor equal to 2, modelling the increasing diameters of successive layers. The time-step response measured by ZARM (316ms) is identical to the theoretical electrical time constant, i.e. the inductance divided by the resistance, L/R (316ms).

ZARM has successfully tested 14 Magnetic Torquers. The prototype above was optimized for PMD by maximizing the electrical time constant and replacing Al housing by non conductive CFRP housing. In conclusion the linearity for a given configuration is well confirmed and the mathematical models are validated.

The magnetic tensor during PMD will be larger due to lower coil resistance at very low temperature.

## 6 CONCLUSIONS

ESA is taking a proactive and innovative approach by preparing some satellites for a possible removal in case they would not have successfully performed the required de-orbiting operations. As part of the Zero Debris approach ESA aims to generalize preparation for removal to all its future missions. The observed long term dynamic evolution of defunct satellites is puzzling, with often high angular rates, very far from an ideal Gravity Gradient lock. The minimisation, prediction and estimation of these angular rates is crucial for the design of the chaser and to confirm the feasibility of these Rendezvous and Capture critical operations.

ESA/Clean Space is preparing a Technical Memorandum providing useful information to the space systems developers community on the specific subject of Magnetic Detumbling performance validation and verification. A preliminary collection of guidelines has been shared in this paper.

At system level, the proposed process is based on High-Fidelity simulations able to perform well thought Monte Carlo campaign and on an analytical framework to correlate simulations, explore driving parameters and guide the simulation campaign.

A Copernicus-like satellite has been defined to illustrate the proposed performance verification process. ESA/ESTEC and ABSpaceConsulting dedicated tools have been used, highlighting the complex competition between Magnetic Detumbling and Solar Radiation Pressure torques.

Some analytical contributions to understand TOPEX/Poseidon dynamic evolution have been shared. At HW level, the verification process undertaken by ZARM Technik on short-circuited Magnetic Torquers under implementation by Copernicus Expansion missions has been described, highlighting the specific approach to carry out electromagnetic measurements with extremely small induced currents and magnetic dipoles

Mastering the Long-Term Dynamic Evolution of Non-Operational Satellites in Low Earth Orbit remains both crucial and extremely complex. The main recommendations for future work are:

Maturation of simulators and validation with observation data; Consolidation of inputs from satellite design (Eddy currents, Solar Array surfaces optical properties, principal axes misalignments, etc.); Development of more powerful Passive Detumbling solutions; Approaches for Solar Array re-orientation in Safe Mode or in case of Disconnect of Non Essential Loads (DNEL).

Collaboration between stakeholders will be instrumental to progress in all areas.

## 7 REFERENCES

### Applicable documents

[AD1] Design for Removal – Interface Requirement Document for LEO missions - ESA-OPS-SC-RD-2023-001 - Jan 2023

### Reference documents

[RD1] A. Benoit et al: Passive magnetic detumbling to enable active debris removal of non-operational satellites in Low Earth Orbit - CEAS Space Volume 13, pages 599–636 (2021)

<https://doi.org/10.1007/s12567-021-00354-8>

[RD2] Soares, T., Benoit, A., Kornienko, A., Bakonyvari, D, et al: Passive rate damping of non-operational satellites in Low Earth Orbit to enable Active Debris Removal – 11<sup>th</sup> International ESA GNC Conference - June 2021

<https://www.esa-gnc.eu/>

[RD3] Benoit, A.: PowerPoint presentation of “Passive rate damping of non-operational satellites in Low Earth Orbit to enable Active Debris Removal” – 11<sup>th</sup> International ESA GNC Conference – 24 June 2021

<https://youtu.be/4DfeSpxvsOw>

- [RD4] Magnetic Damping For Space Vehicles After End-of-life. ESA patent EP19182205  
<https://data.epo.org/publication-server/document?iDocId=6430752&iFormat=0>
- [RD5] Ortiz Gomez, N., Walker, S.J.I., Earth's gravity gradient and eddy currents effects on the rotational dynamics of space debris objects: Envisat case study. Advances in Space Research (2015)  
<https://core.ac.uk/download/pdf/189287881.pdf>
- [RD6] Kucharski, D. et al., Attitude and Spin Period of Space Debris Envisat Measured by Satellite Laser Ranging. IEEE Transactions on Geoscience and Remote Sensing, VOL. 52, NO. 12 (2014).  
[https://www.geoazur.fr/Publis/2014\\_Kucharski\\_GRS.pdf](https://www.geoazur.fr/Publis/2014_Kucharski_GRS.pdf)
- [RD7] Kucharski, D. et al: Spin-up of space debris caused by solar radiation pressure (2017) Proc. 7th European Conference on Space Debris, Darmstadt, Germany, 18–21 April 2017,  
<https://conference.sdo.esoc.esa.int/proceedings/sdc7/paper/395/SDC7-paper395.pdf>
- [RD8] Kucharski, D. et al: Photon Pressure Force on Space Debris TOPEX/Poseidon Measured by Satellite Laser Ranging - Earth and Space Science, 4, 661–668.  
<https://doi.org/10.1002/2017EA000329>
- [RD9] Sommer, S. et al., Temporal analysis of Envisat's rotational motion, Proc. 7th European Conference on Space Debris, Darmstadt, Germany, 18–21 April 2017  
<https://conference.sdo.esoc.esa.int/proceedings/sdc7/paper/437/SDC7-paper437.pdf>
- [RD10] Antreasian, P.G.: Modeling radiation forces acting on TOPEX/Poseidon for precision orbit determination- NASA Technical Memorandum 104564 – 1992  
<https://ntrs.nasa.gov/api/citations/19920019100/downloads/19920019100.pdf>
- [RD11] Dennehy, C, J.: Attitude Determination and Control for the TOPEX Satellite Attitude Determination and Control  
<https://arc.aiaa.org/doi/abs/10.2514/6.1988-4129>
- [RD12] Sagnières, L.: Investigation into the rotational dynamics of the defunct satellite TOPEX/Poseidon  
[https://cdis.nasa.gov/lw21/docs/2018/papers/SessionSD4\\_Sagnieres\\_paper.pdf](https://cdis.nasa.gov/lw21/docs/2018/papers/SessionSD4_Sagnieres_paper.pdf)
- [RD13] Vananti, A. et al: MULTI-SENSOR SPACE OBJECT TRACKING FOR TUMBLING MOTION CHARACTERIZATION - Proc. 2nd NEO and Debris Detection Conference, Darmstadt, Germany, 24-26 January 2023  
<https://conference.sdo.esoc.esa.int/>
- [RD14] Snelling, E.C.: Soft Ferrites Properties and Applications  
[https://ia803405.us.archive.org/1/items/SNELLING\\_SOFT\\_FERRITES\\_1969/SNELLING\\_SOFT-FERRITES\\_1969.pdf](https://ia803405.us.archive.org/1/items/SNELLING_SOFT_FERRITES_1969/SNELLING_SOFT-FERRITES_1969.pdf)
- [RD15] Chen D. et al., Demagnetizing Factors for Cylinders, IEEE Transactions on Magnetics, VOL. 27, NO. 4, JULY 1991  
[Demagnetizing factors for cylinders - Magnetics, IEEE Transactions on \(nist.gov\)](https://ntrs.nasa.gov/api/citations/19910001000/downloads/19910001000.pdf)
- [RD16] Imhülse, T. et al, The Clean Space Solution For The Copernicus Sentinel Expansion – ZARM presentation at COSPAR 2022- 19/07/2022

## Acknowledgements

The work described in this paper was supported by several ESA contracts:

“Support to Active Debris Removal Activities in the frame of Copernicus Expansion Missions”, an ESA contract with ABSpaceConsulting, Ref. 4000136689, and “Characterisation and Optimisation of Short-Circuited Magnetic Torquers for Passive Magnetic Detumbling”, an ESA contract with ZARM Technik, Ref. 4000133200.

Alain Benoit would like to thank Cornelius Dennehy, NASA Technical Fellow for Guidance, Navigation and Control, for having shared TOPEX/Poseidon spacecraft inertia.

## ANNEX: SPINNER EVOLUTION IN QUASI POLAR LOW EARTH ORBIT

The external torque corresponds to:

$$\vec{T} = \vec{T}_{GG} + \vec{T}_{RD} + \vec{T}_{SRP} + \vec{T}_{PMD} (+\vec{T}_{AERO}) \quad (24)$$

In  $\mathcal{R}_{QI}$  shown in Fig. 18 or Fig. 34 the components of the angular momentum are

$$\vec{H} = H \begin{pmatrix} \sin \varphi \cos \theta \\ \sin \varphi \sin \theta \\ \cos \varphi \end{pmatrix}_{\mathcal{R}_{QI}} \quad (25)$$

Assuming that  $\mathcal{R}_{QI}$  is inertial over the considered timeframe, the differential equation governing the long-term evolution of the angular momentum is:

$$\left( \frac{d\vec{H}}{dt} \right)_{\mathcal{R}_{QI}} = \vec{T} = \dot{H} \begin{pmatrix} \sin \varphi \cos \theta \\ \sin \varphi \sin \theta \\ \cos \varphi \end{pmatrix}_{\mathcal{R}_{QI}} + H \begin{pmatrix} \dot{\varphi} \cos \varphi \cos \theta - \dot{\theta} \sin \varphi \sin \theta \\ \dot{\varphi} \cos \varphi \sin \theta + \dot{\theta} \sin \varphi \cos \theta \\ -\dot{\varphi} \sin \varphi \end{pmatrix}_{\mathcal{R}_{QI}} \quad (26)$$

The evolution of the module  $H$  and the direction referred by angles  $\varphi$  and  $\theta$  is:

$$\begin{aligned} (1) \dot{H} \sin \varphi \cos \theta + H(\dot{\varphi} \cos \varphi \cos \theta - \dot{\theta} \sin \varphi \sin \theta) &= T_x \\ (2) \dot{H} \sin \varphi \sin \theta + H(\dot{\varphi} \cos \varphi \sin \theta + \dot{\theta} \sin \varphi \cos \theta) &= T_y \\ (3) \dot{H} \cos \varphi - H \dot{\varphi} \sin \varphi &= T_z \end{aligned} \quad (27)$$

The derivatives  $\dot{H}$ ,  $\dot{\theta}$  and  $\dot{\varphi}$  are obtained by combining these equations:

$$\begin{aligned} \dot{H} &= (T_x \cos \theta + T_y \sin \theta) \sin \varphi + T_z \cos \varphi \\ H \dot{\theta} \sin \varphi &= -T_x \sin \theta + T_y \cos \theta \\ H \dot{\varphi} &= (T_x \cos \theta + T_y \sin \theta) \cos \varphi - T_z \sin \varphi \end{aligned} \quad (28)$$

The orbit-averaged torques created by the Gravity Gradient, the Residual Magnetic Dipole and the Passive Magnetic Detumbling are:

$$\langle \vec{T}_{GG} \rangle_{orbit} = a_{GG} \cos \varphi \sin \varphi \begin{pmatrix} -\sin \theta \\ \cos \theta \\ 0 \end{pmatrix}_{\mathcal{R}_{QI}} \quad \text{with } a_{GG} = \frac{3\omega_0^2}{2} [I_z - \frac{I_x + I_y}{2}] \quad (29)$$

$$\langle \vec{T}_{RD} \rangle_{orbit} = a_{RD} \begin{pmatrix} -\cos \varphi \\ 0 \\ \sin \varphi \cos \theta \end{pmatrix}_{\mathcal{R}_{QI}} \quad \text{with } a_{RD} = \frac{M_{RDz} B_{eq}}{2} \quad (30)$$

$$\langle \vec{T}_{PMD} \rangle_{orbit} = -M \frac{5}{2} B_{eq}^2 \begin{pmatrix} \frac{11}{20} \omega_z \sin \varphi \cos \theta \\ \frac{11}{20} \omega_z \sin \varphi \sin \theta \\ \omega_z \cos \varphi - \frac{9\omega_0}{5} \end{pmatrix}_{\mathcal{R}_{QI}} \quad (31)$$

The torques created by the Solar Radiation Pressure on a lateral Solar Array are first expressed in a Reference Frame attached to the Angular Momentum and transferred into the reference frame  $\mathcal{R}_{QI}$  as shown in Fig. 34:

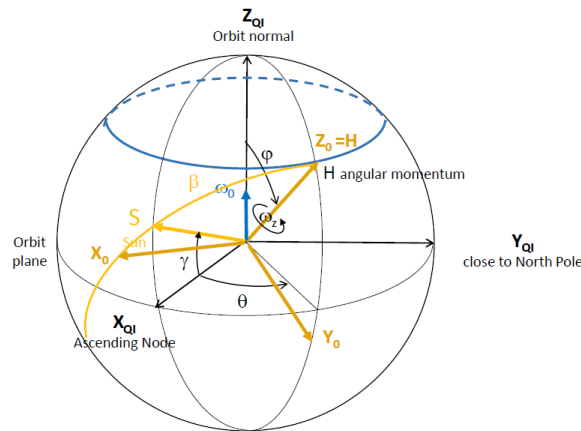


**Fig. 34: Reference frames  $\mathcal{R}_{QI}$  and  $\mathcal{R}_0$**